Feasibility of beer brewing using nano-biocatalyst synthesised from yeast cells and carbon nanotubes

Antony James Higginson

A dissertation submitted to the Faculty of Engineering and the Built Environment, University of the Witwatersrand, in the fulfilment of the requirements for the degree of Master of Science in Engineering

Johannesburg 2010

Declaration

I declare that this dissertation is my own unaided work. It is being submitted to the Degree of Master of Science to the University of the Witwatersrand. It has not been submitted before for any degree or examination to any other university.

……..

..... Day of …….. Year ……

Abstract

The feasibility of utilising a nano-biocatalyst produced using yeast cells and carbon nanotubes for beer fermentation was examined. Carbon nanotubes were used as a site for physical adsorption for the yeast cells. As the use of carbon nanotubes in the production of consumable products is contentious due to the relatively unknown toxicity of carbon nanotubes, a method was developed to anchor the carbon nanotubes to a stainless steel substrate. Direct synthesis of carbon nanotubes on the surface of the stainless steel produced mainly amorphous carbon and reduced the corrosion resistance of the steel when performed at 950^{o}C and hence was disregarded as a method to produce a carrier for yeast cell immobilization. Deposition of nanotubes produced through floating catalyst chemical vapour deposition resulted in a horizontally aligned film of nanotubes. Due to the weak bonds with the surface of the stainless steel, the film degraded in water and was not a viable carrier for yeast cell immobilization. By using pre-deposition of the ferrocene catalyst, prior to carbon nanotube synthesis at 850^{o}C, using acetylene as the carbon source and argon as an inert process gas, vertically aligned carbon nanotubes with diameters ranging from 20 nm to 50 nm formed a densely packed film ranging from 20 µm to 50 µm thick. The resultant vertically aligned carbon nanotube film was then combined with yeast cells and the resultant biocatalyst was tested for feasibility of use in beer fermentation. The biocatalyst was found to be non-viable as the surface coverage of yeast cells, at a yeast loading of less than 0.13 g of yeast per m^2 of biocatalyst, was too low to provide adequate fermentation kinetics. The effect of the cell immobilization on the fermentation products could not be determined due to the low surface coverage of yeast cells on the biocatalyst. Furthermore the carbon nanotube film was found to degrade during fermentation due to hydrodynamic forces and mechanical wear. As this would result in contamination of the final product, the biocatalyst is unsuitable for beverage production. The yeast cells that were in contact with the carbon nanotube film showed morphological changes due to the strong interactions between the carbon nanotubes and the walls of the cells, but continued to divide and grow. As the carbon nanotubes did support cell growth and the cells were adhered strongly to the surface, carbon nanotubes could be used as a biocatalyst in situations where formation of a biofilm is desirous such as in waste water treatment and biomedical scaffolds.

Contents

List of Figures

List of Tables

Acknowledgments

I would like to thank the following for their invaluable assistance:

Professor S. Iyuke

Professor J. Cluett

Dr. C. Yah

The students of the Nano-biotechnology research group

The University of the Witwatersrand Microscope unit

The National Research Foundation and the Institute of Brewing and Distilling for funding

1 Overview of research

1.1 Introduction

Carbon nanotubes were first described by Iijima [1] in 1991 and are an allotropic form of carbon that form long tubes with a very high length to diameter ratio, often being thousands of times longer than wide. Carbon nanotubes are produced in two forms, namely single-walled and multi-walled. Single-walled nanotubes are comprised of a single graphene sheet formed as a cylinder, while multi-walled nanotubes comprise many concentric cylinders and are consequently many times larger than single walled nanotubes. According to IUPAC guidelines for recommended terminology, tubular carbon structures with a diameter greater than 100 nm are termed filamentous carbon [2].

The possible applications for Carbon nanotubes are widely varied. Research is being performed to test the viability of using carbon nanotubes in various applications such as drug carriers [3], in electrical components [4], biosensors [5] and as a scaffold base for tissue engineering [6]. It is however the biological interactions that this research will focus on. Nanotubes provide a unique material for biological applications for three reasons. Firstly the nanotubes are very strong and are not prone to degradation over time. Secondly nanotubes can increase the surface area available for reactions to occur by many times resulting in far faster reactions, and lastly nanotubes exhibit unique electrostatic properties that make biological interactions possible.

Nanotubes may be too small to act as a carrier for cell immobilization on their own, except in the case of cell aggregation [7]. The tendency of nanotubes to form a dense film can be exploited however to provide a carrier for cell immobilization containing millions, if not billions of nanotubes [6]. This film could provide the

properties that are required for a biocatalyst, for example large surface area, which would be impossible to replicate without the use of nanostructured materials. A film of carbon nanotubes also provides excellent properties that are desirable in cell immobilization such as strength and longevity.

1.2 Motivation

Carbon nanotubes provide an interesting carrier for yeast cell immobilization due to their unique structural and electrostatic properties. However for a food or beverage production process the use of freely suspended nanotubes is not feasible due to possible contamination of the final packaged product. Thus a method of production for a carbon nanotube film is required prior to attempts to form a biocatalyst using yeast cells and carbon nanotubes.

This research will show the development of a method to produce a film of carbon nanotubes that will provide a suitable carrier for the immobilization of yeast cells for the Fermentation of beer.

1.3 Research aims

The Aims of this research are twofold, firstly a method will be developed to coat stainless steel wires with carbon nanotubes and the feasibility of using such a coating will be tested in terms of stability of the coating and corrosion resistance. Secondly the application of such a coating for cell immobilization in the field of beer production will be tested in terms of fermentation kinetics of the biocatalyst and general suitability to the process.

1.4 Literature review

1.4.1 Carbon nanotube production through Catalytic Chemical Vapour Deposition

Carbon nanotubes were initially described by Iijima [1] and produced though chemical vapour deposition (CVD) processes by Li et al. [8] in 1996. CVD requires a carbon source, and a metallic catalyst source. Through changing catalyst conditions either single-walled or multi-walled nanotubes can be preferentially grown, for example nickel catalyst will mainly grow multi-walled nanotubes while iron-cobalt alloys grow mainly single walled nanotubes and iron catalysts will form either single or multi-walled nanotubes depending on the size of the catalyst particles [9,10]. The diameter of the nanotubes formed during the reaction is related to the size of the catalyst particle that formed the nucleation point for the nanotube [10].

Carbon nanotubes are formed through the decomposition of a carbon source, which is generally a hydrocarbon such as acetylene. Acetylene undergoes pyrolysis via the process described in Equation 1, which is an autocatalytic reaction at high temperatures [11]. When pyrolysis occurs under controlled conditions the carbon atoms reform to form fullerenes, which is a highly thermodynamically stable form of carbon. If the dehydrogenation of the hydrocarbon occurs rapidly the carbon atoms do not have time to re-order themselves into fullerenes and will form amorphous carbon (soot), which is the least thermodynamically stable form of carbon [12]. If the pyrolysis occurs at a catalyst particle, the carbon diffuses into the catalyst and is deposited as graphene. The continuous deposition of graphene on the surface of the particle results in the formation of a carbon filament [11]. As the rate of diffusion through the catalyst increases with increasing temperature, the rate of graphene deposition increases resulting in an increased rate of nanotube formation [13].

$$C_2H_2 \rightarrow 2C + H_2 \quad (1)$$

The two mechanisms that have been hypothesised for the formation of filamentous carbon structures on a surface are tip growth and extrusion or root growth [11]. In tip growth the filament is attached to the support and the catalyst particle is carried in the tip of the filament, allowing further growth of the filament. The catalyst particle prevents the formation of the hemispherical fullerene cap, but as the catalyst is deactivated the fullerene cap forms encapsulating the catalyst particle [12]. In extrusion the catalyst particle remains attached to the base support, while the filament grows out from the base. The type of growth that occurs depends on the surface-catalyst interactions that occur. If the catalyst is bonded strongly to the surface, root growth occurs. Conversely, if the catalyst particle is loosely bonded to the surface the nanotube will lift the particle off the surface during growth resulting in tip growth. In a floating catalyst CVD synthesis, where the catalyst is not attached to a surface [14,15], the carbon nanotube forms at the catalyst particle and can either be deposited on objects inside the reactor or transported out of the reactor by the process gas.

Ferrocene is an organometallic compound that decomposes to from iron at high temperatures through the reaction given in Equation 2. This decomposition occurs at temperatures as low as 400^{o}C in the presence of a reducing agent, such as hydrogen, however without a reducing agent the decomposition reaction occurs at 827^{o}C [16]. Ferrocene is especially useful as a catalyst source in CCVD due to its low boiling point, which forms in gaseous ferrocene at approximately 250^{o}C, which can then be reacted with a gaseous carbon source.

$$Fe(C_5H_5)_2 \rightarrow Fe + 2C_5H_5 \quad (2)$$

An important factor in the formation of carbon nanotubes is the deactivation of the catalyst. The catalyst is deactivated by deposition of amorphous carbon or large hydrocarbon molecules such as poly-aromatic hydrocarbons (PAHs) [11,12,17,18]. Murphy & Carroll [19] gives the process of acetylene pyrolysis as; dehydrogenation and formation of carbon, hydrogenation to form ethylene and polymerization to form benzene and PAHs. Acetylene is essential in the formation of the initial benzene ring that is an intermediate during PAH formation, thus PAH formation may be prevented by using a carbon source such as methane, which does not lead to PAH formation [17]. The rate at which the dehydrogenation of the hydrocarbon occurs is slowed through the addition of hydrogen. This helps to prevent the formation of amorphous carbon deposits [12]. The addition of an inert process gas, such as argon, reduces the concentration of the hydrocarbon, reducing the amount of amorphous carbon and PAHs that are formed [17]. If the concentration of the hydrocarbon is too high the carbon source becomes saturated, meaning that the catalyst cannot utilise all the carbon to produce carbon nanotubes [20]. In this case the autocatalytic pyrolysis of the hydrocarbon occurs forming soot. Murphy & Carrol [19] states that soot formation can occur in two ways; vapour phase nucleation of carbon and nucleation through deposition of the original hydrocarbon or simple pyrolysis products on a surface. In the case of carbon nanotube synthesis vapour phase nucleation of carbon is the major mechanism of soot formation as hydrocarbons that are deposited on the catalyst surface form carbon filaments as the carbon source decomposes, provided the catalyst has not been deactivated.

1.4.2 Formation of a carbon nanotube film on stainless steel

The formation of a carbon nanotube film on stainless steel has been accomplished in various ways. The carbon nanotubes can be formed externally and deposited on the steel or the nanotubes can be formed directly on the

surface of the wire. Electrophoretic deposition provides a method whereby a horizontally aligned film of carbon nanotubes is deposited on an electrode [21]. The film formed is very dense and less that 1 μm thick. The pores in the film are however too small to provide an increased surface area for yeast cell adsorption due to the dense packing of nanotubes required for film formation. It has been reported that synthesis of carbon nanotubes over stainless steel mesh increases the surface area from 0.01m^2/g to over 40 m^2/g [22], however the usefulness of the increase in surface area for cell immobilization is limited due to the small pore size.

CVD processes can be used to produce nanotube films both through the deposition of fibres and though direct growth on the surface of the material. Nerushev et al. [23] showed that though the deposition of iron catalyst particles on the surface of silicon, a vertically aligned film of nanotubes was obtained. The surface of the film consisted of horizontally aligned tubes in a random arrangement and large cracks formed in the surface of the film. A horizontally aligned film was produced when the catalyst was not deposited on the surface hence the tubes formed externally to the silicon and were deposited horizontally.

Much research has been performed recently into the formation of carbon nanotube films on stainless steel through CVD processes. External formation and deposition on stainless steel requires an external catalyst source and is similar to nanotube deposition on other media [4] in that a horizontally aligned film is formed. The pores in the surface are again too small to allow the entry of yeast cells between the nanotubes. A more attractive option is the direct growth of carbon nanotubes onto the stainless steel substrate. This can either be achieved through deposition of catalyst particles on the surface [24,25,22,26] or, due to the iron content of the steel, through surface preparation and use of the steel itself

as the catalyst source [18,27,28,29,30]. The stainless steel requires pre-treatment prior to nanotube synthesis in order to break down the oxide layer on the surface of the steel as the carbon source cannot diffuse through the oxide layer to reach the catalyst metals, mainly iron, underneath [18].

Production of nanotubes on a stainless steel surface without any surface pre-treatment results in very poor surface coverage [4,18]. As the oxide layer is fully intact during synthesis carbon-catalyst interaction is limited. Some active sites are exposed by the formation of carbides on the stainless steel surface due to reactions between the metals, especially chromium with the carbon present in the steel. The formation of carbide crystals at the grain boundaries causes the oxide layer to crack allowing the carbon source access to catalyst sites, however due to the random nature of the metallic grain structure this results in highly non-uniform fibres to be formed and poor surface coverage [4,18].

The surface pre-treatment can be performed in various ways. Oxidation [18], reduction [4,28,31], acid etching [4,29,30] or a combination of measures [18,27]. Oxidation increases the thickness of the oxide layer resulting in cracks forming, allowing the carbon source access to the catalyst metals in a similar manner to carbide formation but with greater success. Oxidation can be performed by heating, burning, laser oxidation or through “pickling” with nitric acid. If oxidation occurs rapidly, for example though burning large cracks will form and pieces of the surface will flake off. If the thickening is gradual however, the oxide will remain attached to the surface of the metal, modifying the grain structure of the surface and provide many active sites for carbon nanotube growth [18].

Reduction is performed using a reducing agent such as H_2 gas to reduce the oxide layer to the constituent metals, which can then interact with the carbon source.

If reduction is performed without prior thickening of the oxide layer the steel surface will maintain its original grain structure and hence the nanotubes formed will be highly non uniform [18,31,32]. Thickening the oxide layer will result in a modified grain structure and once reduced will provide for production of uniform nanotubes over a large proportion of the steel surface [18].

The surface can also be modified through the use of strong acids such as HCl and H_2SO_4 that will react with the surface of the steel. The use of strong acids not only changes the structure of the steel but also the distribution of the constituent metals [30]. The use of strong acids leaches chromium from the surface of the metal increasing the relative amount of iron on the surface. The removal of chromium from the surface of the stainless steel has a dual purpose as the lower chromium concentration prevents the oxide layer from reforming to its original thickness as well as increasing the presence of the major catalyst source, iron, on the surface. Hence acid preparation of the surface provides for excellent uniformity and surface coverage

1.4.3 Carbon induced stainless steel sensitisation

The oxide film that forms on the surface of stainless steel is comprised mainly of chromium III oxide, Cr_2O_3 [33]. This protective coating forms naturally in air due to the high concentration of chromium in the surface layer of stainless steels and the high affinity of chromium for oxygen. At temperatures between 650^{o}C and 850^{o}C the chromium will preferentially form carbides at high carbon concentrations [34]. The carbides are usually in the form of Cr_7C_3 or $Cr_{23}C_6$, hence a very large amount of chromium can be contained by a small amount of carbon. Steel naturally contains small amounts of carbon thus stainless steel is susceptible to high temperature sensitization. This is known as inter-granular

corrosion, which is caused by chromium carbide deposits forming at the grain boundaries. This results in the depletion of chromium from the surface layer of the steel, which prevents the formation of the oxide layer, exposing the iron in the steel to oxidation. The carbon content of the steel can be increased by exposing the steel to an atmosphere with high carbon activity at high temperatures [35]. The rate at which carbon diffuses into the steel increases as the temperature increases, the increased carbon concentration in the steel results in faster carbide formation.

1.4.4 Fermentation process in beer production

The main fermentation process used in beer brewing is the conversion of carbohydrates into ethanol and carbon dioxide. Theoretically under anaerobic conditions 0.511g of ethanol can be produced per g carbohydrate [34] due to the stoichiometry of the reaction. This yield is not actually achievable even under perfect conditions as some of the carbohydrate will be used by the yeast during respiration and to reproduce. Blair & Pigman [36] showed that the actual yield lies between 85-92% of the theoretical yield.

Carbohydrates in the wort are broken down during glycolysis in the cell cytoplasm through the Embden-Meyerhof pathway, producing ATP [37]. Mitochondria organelles are responsible for aerobic metabolism, where ATP is produced under aerobic conditions. The dissolved oxygen content has a major effect on the yeast as it determines the form of respirative growth that the yeast cell will use. The three forms of growth are aerobic growth, where the dissolved oxygen content is high, which gives the lowest ethanol yield, yet the most biomass growth. Anaerobic growth, which occurs at low oxygen levels, results in a much higher ethanol yield but lower rate of biomass growth. Finally

oxidoreductive growth occurs at very high carbohydrate concentrations, this again results in a lower ethanol yield than aerobic respirative growth, however the biomass growth rate is as much as 50% higher [38].The metabolic pathway for ethanol production by *Saccharomyces cerevisiae* is shown in Figure 2.1 [39].

The most important product after ethanol and CO_2 is glycerol, which is produced at approximately 1% (v/v). Various stresses can cause the cell to produce glycerol from dihydroxyacetone, an intermediate product in the intracellular process, these stresses include low pH, high osmotic pressure and interruption of the

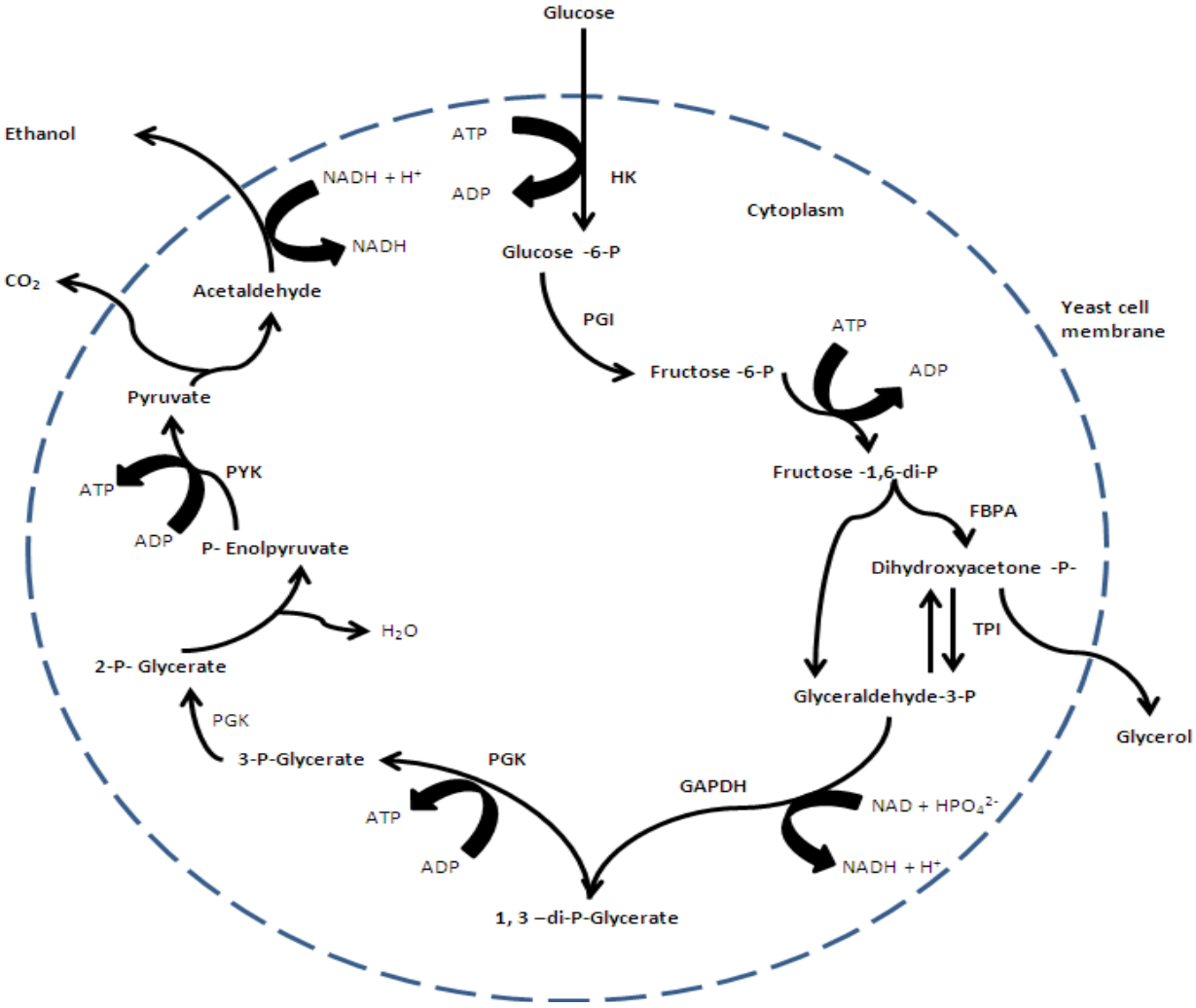

Figure 2.1. Metabolic pathway of *Saccharomyces cerevisiae* for production of alcohol modified from Bai et al. [39]

intracellular process [39]. In addition to CO_2, ethanol and glycerol organic acids are a further product of carbohydrate metabolism. Other metabolic processes in the yeast cell are given as lipid metabolism, amino acid metabolism and carbohydrate/amino acid metabolism. These processes produce various compounds such as esters, short chain fatty acids, higher alcohols, keto acids, SO_2, H_2S, diacetyl, acetonin as well as 2,3-butanediol and many other products in extremely low concentrations that flavour the beer. While the other metabolic processes in the cell do provide flavour to the beer it is preferable to reduce the rate at which these processes occur as the balance of flavours found in beer will be adversely affected.

1.4.5 Immobilization of yeast cells in beer fermentation

The function of yeast immobilization is to provide bulk to the cells to prevent the cells being removed from a system due to fluid flow or other forces. Kourkoutas et al. lists the various mechanisms of cell immobilization as; immobilization on a solid carrier surface, entrapment within a porous matrix, cell flocculation and mechanical containment behind a barrier [40].

Entrapment of cells in a porous matrix is often performed using gels such as Ca-Alginate which allow transport of substances such as sugars and proteins but do not allow immobilized cells to exit the matrix. Cells however reproduce and the new cells can be released from the matrix into the fermentation medium. Immobilization through containment prevents the cells from leaving the carrier by using microfiltration membranes to separate the cells from the fermentation medium. Neither of these mechanisms of immobilization is applicable to biocatalyst production using carbon nanotubes.

The mechanisms of interest when producing a biocatalyst using carbon nanotubes are flocculation and surface immobilization. Due to the length and charge of carbon nanotube it may be possible to utilise the tubes as a cross linking mechanism to accelerate cell flocculation in yeast cells. Surface immobilization is also interesting in terms of biocatalyst production using carbon nanotubes as a film of carbon nanotubes has an incredibly large surface area compared to the original surface. The increase in surface area in most cases is not useful as the pores are far too small to allow yeast cells access, however vertically aligned nanotubes could provide an increase in the surface area while allowing yeast cells access.

For immobilization supports to be used in a food or beverage application the carrier should satisfy several criteria [40,41,42]:

1) The carrier must have a large surface area and provide sites for cells to be immobilized
2) The carrier should be exceptionally stable during fermentation and maintain suitable operation over extended periods of time.
3) The physiology and metabolism of the cells must not be adversely affected by the carrier
4) Exchange of substrates and products around the cells must be uniform to prevent build up or exhaustion
5) The process used to immobilize the cells must be easy to perform, economically viable and possible to scale up for industrial applications
6) The carrier must not contaminate the product in any way and be acceptable to consumers

Many substrates have been used effectively to immobilize yeast for alcoholic fermentations. Inorganic examples include calcium alginate particles, glass

beads, diatomaceous earth [43], PVA pellets [44], stainless steel [45] and many others. Organic media can also be utilised to immobilize the yeast cells for fermentation. Some examples of organic immobilization media include orange peel [46], brewer's spent grains [47] , watermelon rind [48], and sorghum bagasse [49].

1.4.6 Mathematical modelling of yeast growth

Many of the models used to predict the growth of yeast are derived from the Monod model, which is given as Equation 3 [50], where X is the biomass concentration, t is the time, μ_{max} is the maximum growth rate, S is the substrate concentration and K_{sx} is the growth constant. The Monod model is based on Michaelis Menten kinetics, and gives the yeast growth, substrate consumption and ethanol production as non-linear differential equations. As the solution to the equations is non-linear, the regression to find the constants is difficult and applicable only to the set of conditions used in the experiments. The model cannot predict the growth of yeast expect under substrate limiting conditions, for example if the oxygen concentration is not constant the model fails to predict the growth of yeast, as when the oxygen concentration tends towards zero the aerobic growth of the yeast will stop. The Monod model is substrate limiting hence will tend towards zero as the substrate concentration goes to zero.

$$\frac{dx}{dt} = \mu_{max} \ \frac{S}{K_{sx}+S} \ x \qquad 3$$

More simplistic models can be used to predict the growth of yeast, including linear, exponential and logistic growth [51]. As logistic growth describes the traditional progression of microbial growth through lag, exponential and stationary phases, it can be used to model the growth of yeast accurately. The rate of logistic growth is given in Equation 4, where μ is the growth constant and X_0 and X_m are the initial and maximum yeast concentrations respectively in g/l.

The constants that are obtained from the data when fitting the logistic curve are only applicable to the conditions of the experiments from which the data were obtained. Analysis of the data can be performed to determine the ethanol yield, Y_P, and the biomass yield, Y_X. These values show the relative production of biomass and ethanol compared to carbohydrate utilisation.

$$X = \frac{X_M}{1+((X_0\ \ X_M)-1)e^{-\mu t}} \quad 4$$

$$Y_P = \frac{P}{S_0-S} \quad 5$$

$$Y_X = \frac{X-X_0}{S_0-S} \quad 6$$

1.4.7 Forces applicable in cell attachment to a surface

The long range (5-100 nm) forces applicable to cell immobilization are described as being an electrostatic force governed by the surface charge of the cells and van der Waals forces. These forces are often modelled using the Derjaguin-Landau-Verwey-Overbeek (DLVO) theory [52]. This models the overall forces to be additive between an attractive van der Waals force and a repulsive electrostatic force. Unfortunately there is currently no model to describe an attractive electrostatic force. The DLVO predicts an energy barrier that could prevent the cell from gaining access to the surface. If the energy barrier is greater than the energy of the cells adhesion will be prevented, if however the energy of the cells is large enough to cross the energy barrier the cells may be able to adhere to the surface [53]. The strength of the energy barrier decreases with increasing electrolyte concentration hence many researchers have found that in fermentation conditions, where the ionic strength is greater than 10 nM, the energy barrier is negligible. Once the cells reach the surface of the carrier

hydration forces become important short range forces allowing cells to adhere to the surface.

The stages in cell adsorption can be described as follows [54]:

1) Cells are transported from the fermentation medium to the surface of the carrier
2) Cells become attached to the surface, this phase of attachment is reversible and is governed by the forces applied to the cells
3) Synthesis of biopolymers is performed by the cells, which anchors the cells to the surface, biofilm formation.

In yeast cells biopolymers are produced during cell flocculation, hence cells that have flocculated or starved of nourishment have been found to attach more readily to the surface of carriers [45].

Brànyik et al. [53] state the interactions between yeast cells and a carrier take differing forms. The forces mentioned above lead to cell-carrier attachment whereby cells attach to the surface of the carrier. Cell-carrier adsorption occurs when cells enter sheltered cavities in the surface of the carrier. This has a dual effect of increasing the available surface area for cell attachment and protecting the cells from shear forces that would otherwise cause the cells to detach from the carrier surface. Cell-cell attachment occurs when a cell that is attached to the surface comes into contact with a free cell. The free cell can attach to the immobilized cell using biopolymers, this is especially common in the case of cell carrier adsorption where the close contact between cells and lack of shear forces increases the interaction between cells.

1.4.8 Effect of carbon nanotubes on cell growth and toxicity

Although carbon nanotubes have successfully been used in biological applications in the past, especially in enzyme and protein immobilization, whole cell immobilization for fermentation using carbon nanotubes is rare. However various types of cells have been grown or immobilized on carbon nanotubes for other applications. These include the use of carbon nanotube films as medical scaffolds and the use of CNT elimination of pathogens.

Nanotubes, functionalized with mannose and galactose, were found to form aggregates with *Bacillus anthracis* (Anthrax) spores [55]. The nanotubes were found to provide a suitable scaffold to aggregate the spores however the binding forces were supplied by the carbohydrate side chains rather than the nanotubes themselves. *Bacillus subtilus* spores were found to have a higher adsorption rate onto carbon nanotube aggregates in comparison to activated carbon and ceramic materials [7]. The aggregates were not formed for immobilization and fermentation however and were meant for use in biosensors.

The capture of *Streptococcus mutans* by carbon nanotubes was reported by Akasaka & Watari [56]. It was found that, due to the flexibility of carbon nanotubes, the nanotubes would wrap around the cells causing precipitation. However the research showed that larger diameter multi-walled carbon nanotubes, at approximately 200 nm, were not adequately flexible to wrap around the cells and hence did not capture the bacterial cells as efficiently as the thinner, more flexible nanotubes.

The use of carbon nanotube films as medical scaffolds shows that a biocatalyst could be produced using carbon nanotubes and yeast cells. Correa-Duarte et al.

[6] showed that mouse fibroblasts could be grown on three dimensional multi-walled carbon nanotube networks, without the fibroblasts experiencing any cytotoxic effects. Hu et al. [57] showed that neuronal cells grew on carbon nanotubes as well as on functionalised nanotubes. The research however showed that the morphology of the cells was affected by the charge of the nanotube, with a positive charge resulting in much longer neurites than either neutrally or negatively charged carbon nanotubes. The growth of osteoblasts on a carbon nanotube scaffold was recorded by Zanello et al. [58], the research showed that a neutrally charged carbon nanotube scaffold allowed for the greatest growth, however all cells that were in contact with the nanotubes grew less quickly than the control samples. Furthermore the research showed that the osteoblasts in contact with the multi-walled carbon nanotubes had a greatly changed morphology as a result. The changes in morphology were due to the interaction between the carbon nanotubes and the plasma membrane of the cells.

There are concerns over the toxicity of carbon nanotubes especially pulmonary toxicity due to their fibrous nature. Studies have found that nanotubes are more toxic than carbon black upon inhalation [59], however other studies have been inconclusive [60]. On a microscopic scale the toxicity of nanotubes is based the geometry of the tubes and possible interactions with the cell membrane. Kang et al. [61] state that the main mechanisms of nanotube cytotoxicity are: oxidative stress, metal toxicity and physical piercing. Oxidative stress is caused through chemical interactions between the nanotubes and the bacterial cell membrane. Metal toxicity is caused by residual catalyst particles within the nanotubes leaching into the surrounding environment and eventually cells. Physical piercing occurs when the nanotube acts as a needle due to the shape piercing the cell membrane and causing the intracellular contents to spill out. The major cause of cell death seems to be the piercing mechanism, explaining the strong

antimicrobial activity of single walled nanotubes against Escherichia coli [61] and Alveolar Macrophages [62], and the reduced toxicity of multi-walled nanotubes and fullerene (C_{60}) against Alveolar Macrophages [62]. The cytotoxic effect of carbon nanotubes seems to be reduced by the presence of a cell wall in addition to a cell membrane..

1.4.9 Yeast cell immobilization on carbon nanotubes

Due to the unique structure of carbon nanotubes and the range of composite materials that can be produced, nanotubes could be used for all the immobilization methods mentioned in section 1.4.5 except for entrapment of cells within a porous matrix. Cell aggregation or flocculation however requires freely suspended nanotubes that might contaminate the product and hence cannot be used for food or beverage production. Mechanical containment behind a barrier would require complex arrangement of the nanotubes, hence attachment to a solid carrier surface, coated with nanotubes, is the most viable option.

Cell immobilization on a solid carrier surface has the major advantage that the attachment of cells is a spontaneous process that occurs during the biological reaction [49]. Hence for beer brewing the biocatalyst surface only needs to be placed in the fermenting wort and the yeast cells will attach to the surface. Assuming the biocatalyst achieves adequate yeast cell loading it can then be used as the starter culture for subsequent fermentations from which the fermentation kinetics can be obtained. However nanotubes have not been used in fermentation before.

2 Experimental methods

2.1 Carbon nanotube production apparatus

The carbon nanotubes were produced through the swirled floating catalyst chemical vapour deposition method described by Afolabi et al. [15]. The reactor is composed of a 5 cm inner diameter quartz reactor, 100 cm in length placed vertically in a furnace where the temperature is set via the control unit. Gasses are fed into the reactor via a vaporization chamber at the bottom of the reactor which is heated by a heating plate. The temperature of the heating plate is set at 350^{o}C. The flowrate of the gasses entering the reactor are controlled and measured by Cole-Parmer n082-03 rotameters using a glass float. The calibration charts for the rotameters can be found in Appendix A. Gasses exit the system through pipes at the top of the reactor.

The direct synthesis of nanotubes without the addition of an external catalyst was performed by placing five 10 cm lengths of 0.9 mm diameter type 304 stainless steel wire 50 cm from the bottom of the reactor supported by quartz wool. The reactor was then sealed and flushed with argon at a flowrate of 647.3 cm^{3}/min for 15 minutes to remove the oxygen from the system. The furnace was then heated to the desired reaction temperature, after which the synthesis gasses were added and allowed to react for 15 minutes. The reaction conditions used are as follows

1) No wire pre-treatment. Furnace at 600^{o}C, synthesis gas: acetylene 260.9 cm^{3}/min, argon 572.9 cm^{3}/min
2) No wire pre-treatment. Furnace at 850^{o}C, synthesis gas: acetylene 260.9 cm^{3}/min, argon 572.9 cm^{3}/min
3) No wire pre-treatment. Furnace at 950^{o}C, synthesis gas: acetylene 260.9 cm^{3}/min and argon 572.9 cm^{3}/min

4) Oxide layer reduction at 800^{o}C using Hydrogen 807.8 cm^{3}/min and argon 455.6 cm^{3}/min, Furnace at 950^{o}C, synthesis gas: acetylene 260.9 cm^{3}/min, argon 455.6 cm^{3}/min and hydrogen 905.6 cm^{3}/min

The final method that was used in an attempt to synthesise carbon nanotubes on stainless steel without the addition of an external catalyst was based on the method of Baddour et al. [29]. The wires were first acid etched for 10 min in a 15% solution of hydrochloric acid. The wires were then rinsed using distilled water and allowed to dry. The wires were then placed in the reactor, as in the previous experiments, 50 cm from the bottom of the reactor supported by quartz wool. The reactor was then sealed and purged using argon at a flowrate of 647.3 cm^{3}/min for 15 min. the furnace was then heated to 850^{o}C and left for 30 min. The reactor was the allowed to cool to 700^{o}C where the synthesis gases were added; argon 647.3 cm^{3}/min and acetylene at 169.8 cm^{3}/min.

The reactor was then flushed with argon and allowed to cool. The wires were removed once the reactor had cooled to room temperature and stored in a sealed container.

Production of carbon nanotubes using an external catalyst source required the addition of ferrocene to the system. In this case five 10 cm lengths of type 304 stainless steel wire were placed 25 cm from the bottom of the reactor supported by quartz wool. 5 g of ferrocene powder was also placed on the quartz wool support. The reactor was then flushed with argon at a flowrate of 647.3 cm^{3}/min for 15 minutes. The furnace was then heated to 850^{o}C. For catalyst pre-deposition, argon was then passed through the reactor at a flowrate of 647.3 cm^{3}/min for 10 minutes. The synthesis gasses were then added to the system in the following conditions.

1. Furnace at 850^{o}C, no catalyst pre-deposition, synthesis gas: acetylene at 406.3 cm^{3}/min

2. Furnace at 850^{o}C, catalyst pre-deposition, synthesis gas: none
3. Furnace at 850^{o}C, catalyst pre-deposition, synthesis gas: acetylene at 406.3 cm^{3}/min, argon at 332.1 cm^{3}/min

The reactor was then flushed with argon of and allowed to cool. The wires were removed once the reactor had cooled to room temperature and stored in a sealed container.

2.2 Washing and corrosion tests

The washing of wire samples was performed in 500ml beakers, filled with 300ml of distilled water and placed in a rotary shaker at 100 rpm for 4 hours. This time was chosen as it was the time taken for the air bubbles surrounding the wires to dissipate. The wire samples were then removed from the water and dried in an oven at 75^{o}C for 4 hours.

Immersion tests were performed to test the corrosion resistance of the various wire samples. To test the oxidation resistance a 2 cm lengths of wire were placed in 250ml conical flask with 100ml of distilled water. After 24 hours the wire samples were removed and dried in an oven at 75^{o}C for 4 hours. The wire samples were then visually inspected for signs of iron oxide, which presented as orange-red deposits on the surface of the samples. The resistance of wire samples to acidic corrosion was tested by placing 2 cm lengths of wire in 150ml of a 38% solution of sulphuric acid. The 38% solution of H_2SO_4 was produced by mixing 50ml of 72% H_2SO_4 with 100ml of distilled water. The solution was then placed in 250ml conical flasks with a sample of wire. After 24 hours the wires were rinsed with distilled water and dried in an oven at 75^{o}C for 4 hours. The mass of each wire sample was measured before and after the corrosion test to determine the mass that was lost due to corrosion.

2.3 Immobilization of yeast cells on carbon nanotubes

Yeast cell immobilization was carried out by immersing 10 cm lengths of wire in actively fermenting medium of yeast cells and malt extract. The wort was produced by mixing 120 g of dried malt extract in 1000 ml of distilled water which was then autoclaved at 121^{o}C for 15 min. the autoclaved extract mixture was then cooled and filtered using a Millipore aseptic filter housing and Whatman cellulose nitrate sterile membrane filters. The filter pore size was 0.45 µm which removed particulate matter from the extract mixture. The pH of the solution was then adjusted to approximately 4.2 using phosphoric acid. 170 ml of the filtered extract was then placed in 250 ml conical flasks, which were stopped with cotton wool and covered by aluminium foil, and placed in a rotary shaker at 23^{o}C and 100 rpm for 4 hours to reach the desired temperature.

Dried Fermentis S-04, species *Saccharomyces cerevisiae*, was used as the yeast for the immobilization experiments. The data sheet supplied by Fermentis may be seen in Appendix B. The dried yeast was first rehydrated by mixing 2 g of dried yeast with 20 ml of distilled water in a 25 ml conical flask. The flask was then placed in a rotary shaker at 23^{o}C and 100 rpm for 4 hours. The yeast was then inoculated by transferring the yeast slurry from the 25 ml conical flask to the 250 ml conical flasks using a mechanical pipette. The experiments performed were as follows: 4 ml of slurry and CNT coated wire, 2 ml of slurry and CNT coated wire, 1 ml of slurry and CNT coated wire, 1ml of slurry and uncoated wire. All equipment used in the immobilization experiments was autoclaved at 121^{o}C for 15 min prior to use.

Samples were collected from the flasks at intervals by removing 10 ml of the medium using a mechanical pipette. The samples were then tested for pH, absorbance and 5 ml of each sample was filtered using a Millipore aseptic filter

housing and Whatman cellulose nitrate sterile membrane filters, pore size 0.45 µm, and frozen for analysis by high performance liquid chromatography. Samples of the wire were obtained by removing the wires from the medium using forceps and cutting off a 1 cm section from the end of the wire. The wire was then rinsed by dipping into distilled water and dried in an oven at 80^{o}C for 40 min, the wires were then placed in sterilized sample jars until microscopic analysis was performed.

2.4 Analytical methods

Microscopic analyses were carried out using a JEOL 100S electron microscope. Samples were mounted onto aluminium stages using graphite paste and were observed in the microscope. No coating was required due to the presence of conductive materials on the surface of the samples. High magnification scanning electron microscope images were taken using a FEI Quanta 400F Environmental Scanning Electron Microscope (ESEM). The samples were coated using gold-palladium shading to increase the conductivity when viewing yeast cells.

High performance liquid chromatography (HPLC) was performed using an Agilent 1200 series HPLC using a quaternary pump, vacuum degasser, auto-sampler and refractive index detector. The column used was a Biorad Fermentation monitoring column with a guard column. The mobile phase used was a 0.001M solution of H_2SO_4 at a flowrate of 0.8 ml/min. The column temperature was maintained at 60^{o}C using a Chromtec column housing. The HPLC results were analysed using Agilent Chemstation software, and calibration of the HPLC was performed as shown in Appendix C.

The yeast cell concentration in the fermenting broth was determined by measurement of the absorbance of the broth. The absorbance was determined using a Unico uv/vis double beam spectrophotometer. The absorbance was determined for a sample by mixing 1 ml of the fermenting broth with 3 ml of distilled water in a cuvette, a reference sample was also made in a similar manner however using broth that had been filtered to remove the yeast cells mixed with distilled water. The absorbance of the fermenting broth was determined relative to the reference sample to obtain the effect of the yeast cells on the absorbance. The yeast cell concentration was calculated by comparing the absorbance to a calibration curve that had been developed using known yeast cell concentrations. The calibration calculations and methodology may be found in Appendix D.

3 Results and Discussion

3.1 Direct synthesis of carbon nanotubes on stainless steel

Figure 3.1 A shows the surface of the stainless steel wire prior to any reaction or treatment. Striation can clearly be seen on the surface of the wire and are remnants of the production process. Aside from the parallel striation it can be seen that there are no horizontal cracks in the surface of the wire.

The initial attempts to produce a carbon nanotube film without the addition of an external catalyst were performed by using process gas composed of acetylene at 260.9 cm^3/min and argon at 572.9 cm^3/min at various temperatures. Figure 3.2 B shows the surface of a wire that had been heated to 600^oC and exposed to the process gas for 15 minutes. The surface shows no growth of carbon filaments

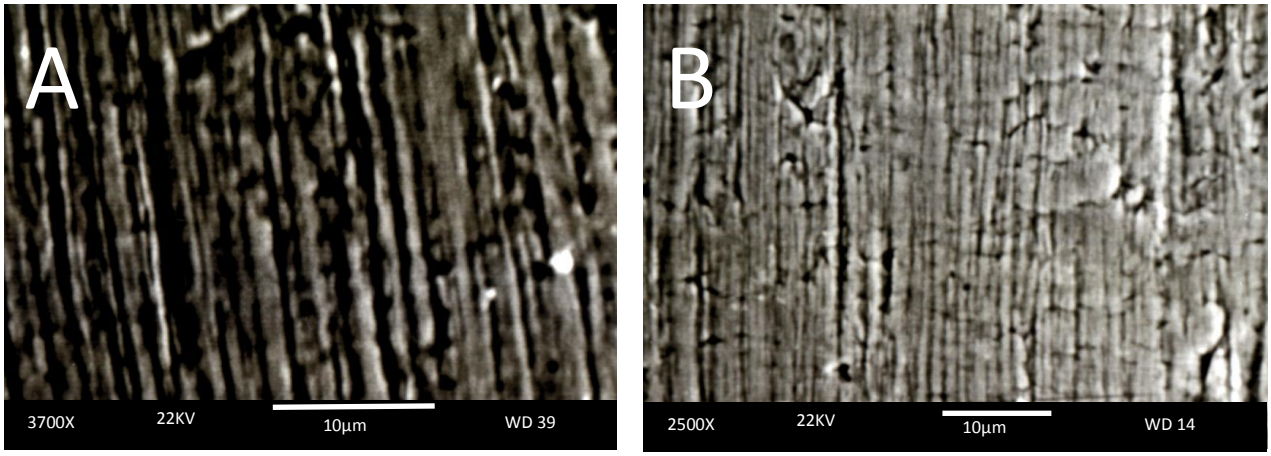

Figure 3.1: SEM images of stainless steel wire samples (A): Wire surface prior to any treatment, (B): Wire after carbon nanotube synthesis reaction at 600^oC without the addition of an external catalyst

however the surface shows horizontal cracks in addition to the striations that could be seen in the plain wire surface. With the reaction at 600^oC there is some deposition of amorphous carbon onto the surface of the wire, as illustrated in Figure 3.3 A.

Using the same process gas at 850^{o}C for 15 min produced large filaments, with a diameter greater than 1 µm, on the surface of the stainless steel. The surface coverage of filaments was negligible and the majority of the surface was coated with amorphous carbon, as shown by Figure 3.3 B and C.

Performing carbon nanotube synthesis on stainless steel at 950^{o}C caused severe damage to the surface of the wire, shown in Figure 3.2 D and Figure 3.3 A, B, C and D. The addition of hydrogen to the process gas did not reduce the damage to the surface of the wire, however the deposition of carbon nanoballs in addition to the deposition of amorphous carbon that was also visible in the wires exposed

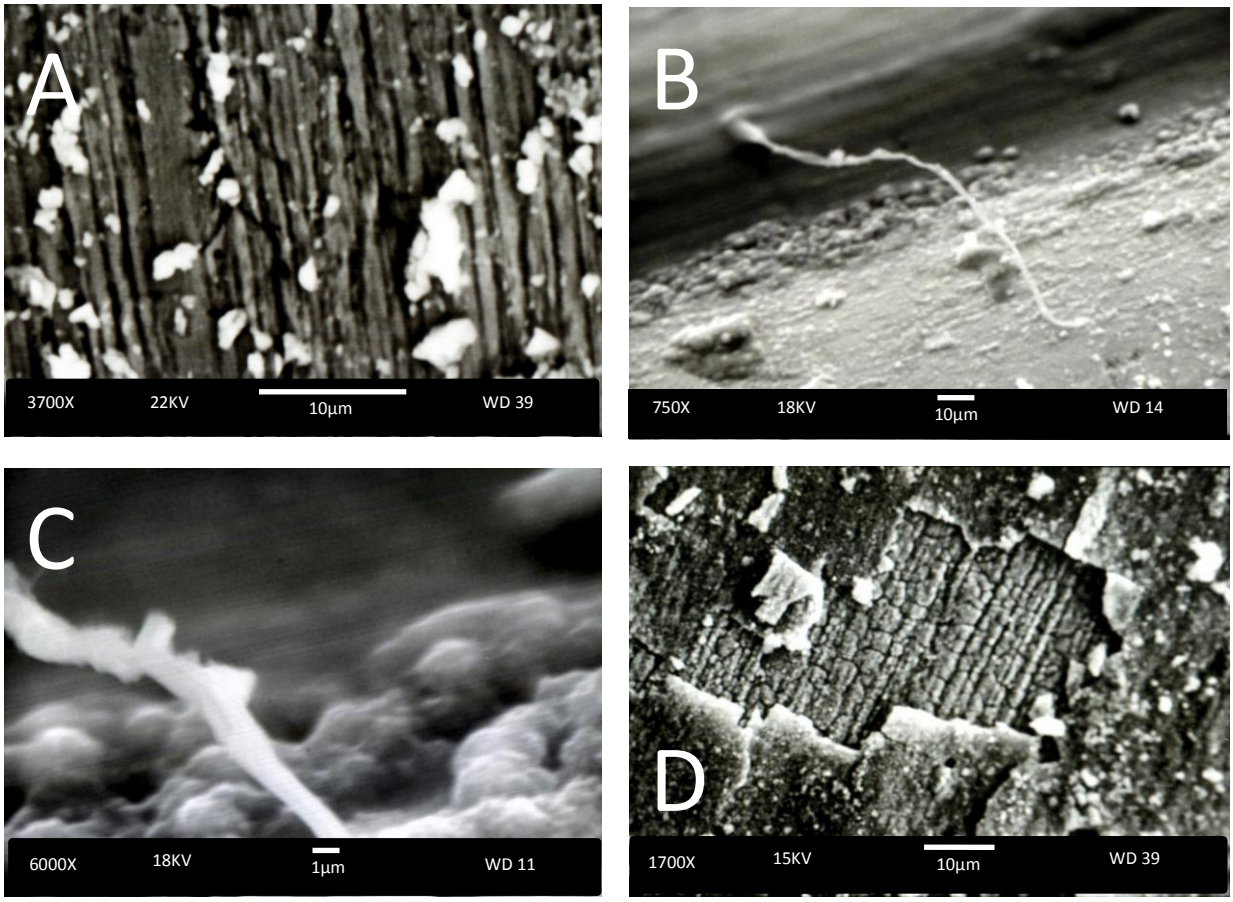

Figure 3.2: Stainless steel wire after carbon nanotube synthesis without the addition of an external catalyst at (A): 600^{o}C, (B): 850^{o}C showing filamentous carbon growth, (C): 850^{o}C showing defects in carbon filament, (D): 950^{o}C showing damage to surface

to process gas without hydrogen. This is consistent with the findings of van der Wal & Hall [18], whereby the addition of hydrogen reduces the formation of amorphous carbon deposits. In the absence of a suitable catalyst this results in the formation of carbon nanoballs rather than nanotubes.

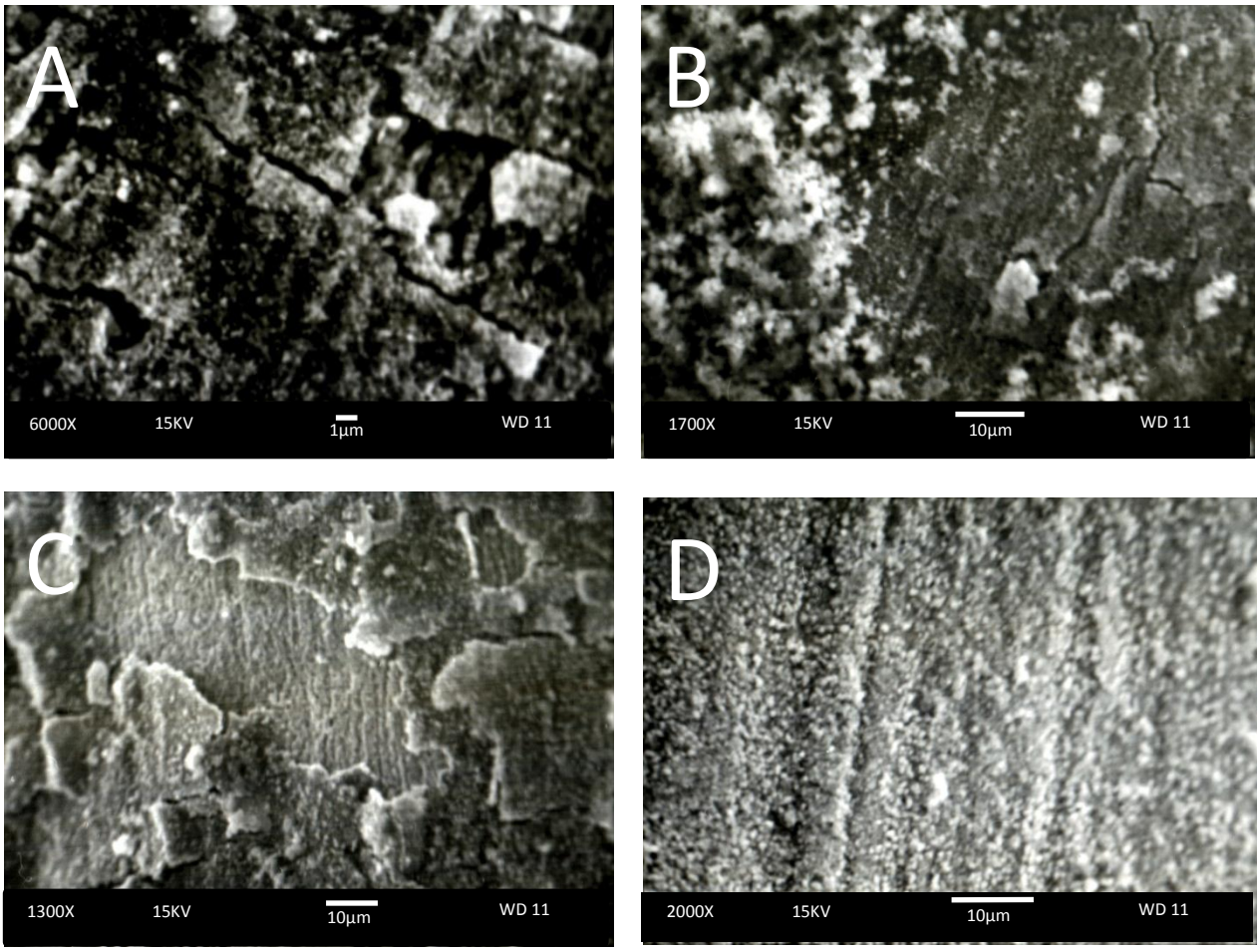

Figure 3.3: Stainless steel wire after carbon nanotube synthesis without the addition of an external catalyst at A: 950^{o}C, (B): 950^{o}C after 24 hour immersion in distilled water, (C): 950^{o}C with the addition of hydrogen, (D): 950^{o}C with the addition of hydrogen showing granular deposits on wire surface

The final method used to produce a nanotube film without the use of an external catalyst involved three stages. The steel was prepared initially through etching with 15% hydrochloric acid. The acid did not drastically alter the surface of the steel however, as shown in Figure 3.4 A, augmented the surface striations caused by the production process. The synthesis of nanotubes involved a two stage

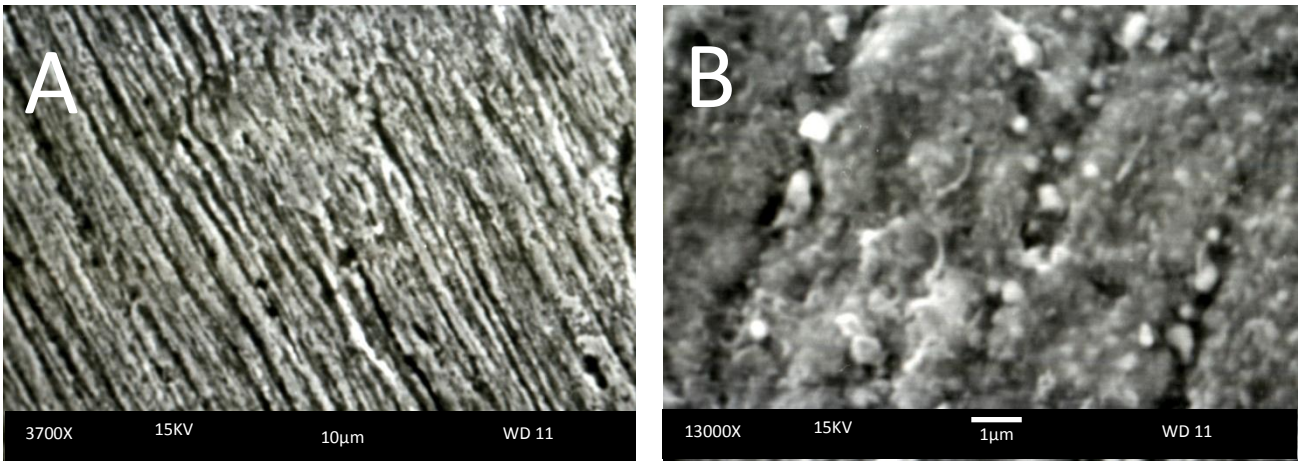

Figure 3.4: Stainless steel wire; (A): after reaction with 15% HCL for 15 min, (B): after synthesis at 700^{o}C

heating process. The wires were heated to 850^{o}C to break down the oxide layer of the wires. The wires were then cooled to 700^{o}C and exposed to process gas of argon at 647.3 cm^{3}/min and acetylene at 169.8 cm^{3}/min. This method did not result in any nanotube growth, with only amorphous carbon deposits on the surface as can be seen in Figure 3.4 B.

The overall lack of nanotube production when using synthesis without the addition of an external catalyst can be explained by the lack of active catalyst sites for nanotube formation. This is mainly due to the presence of the chromium rich oxide layer, however treatment with sulphuric acid and reduction using hydrogen should have exposed active catalyst sites for nanotube growth. Catalyst sites are deactivated by the deposition of amorphous carbon [18]. Amorphous carbon deposits were found on all wires after the synthesis reaction with the exception of the reaction at 600^{o}C. Carbon deposits deactivate the catalyst sites and prevent the formation of nanotubes. In the absence of an external catalyst the steel surface is the only site where nanotube synthesis can occur. The wires only supply a surface area of 2.8 cm^{2} in a reactor volume of 1.96 dm^{3}. The residence times of the synthesis gas were greater than 30 seconds in all cases, meaning that the autocatalytic pyrolysis of acetylene would occur, causing

the amorphous carbon deposits that were visible in all cases where no external catalyst was used.

3.2 Production of a carbon nanotubes on stainless steel through the addition of an external catalyst

Carbon nanotubes were produced via chemical vapour deposition through the pyrolisis of acetylene using 5 g of ferrocene catalyst powder at 850^{o}C. The nanotube synthesis was performed without pre-deposition of the catalyst on the stainless steel wires and using pure acetylene, at a flowrate of 406.3 cm^{3}/min. This production method was found to produce nanotubes of highly variable size and many impurities such as nanoballs and non-tubular carbon structures (NTCs). Figure 3.5 A shows SEM analysis of carbon deposits produced through this process. Carbon nanotubes are visible on the surface of the film however there are many NTCs that were deposited on the surface. After the wires were washed in distilled water the impurities and loose nanotubes were mostly removed leaving a horizontally aligned film of nanotubes, as shown by Figure 3.5 B and C. The horizontal alignment and random arrangement of the film indicates that the nanotubes were formed on floating catalyst particles and then deposited onto the surface of the stainless steel. Figure 3.5 D shows the film flaking off from the surface of the stainless steel after 3 cycles of washing in distilled water and drying at 100^{o}C, the exposed surface shows only minimal damage in comparison to the direct synthesis reactions performed at 950^{o}C.

The nanotube synthesis process was modified by the addition of a catalyst pre-deposition step using argon carrier gas at 647.3 cm^{3}/min for 10 min at 850^{o}C. The nanotube synthesis then proceeded using acetylene at a flowrate of 406.3 cm3/min with argon carrier gas at a flowrate 332.1 cm^{3}/min. The gas mixture was fed into the reactor for 15 min, after which the reactor was purged using

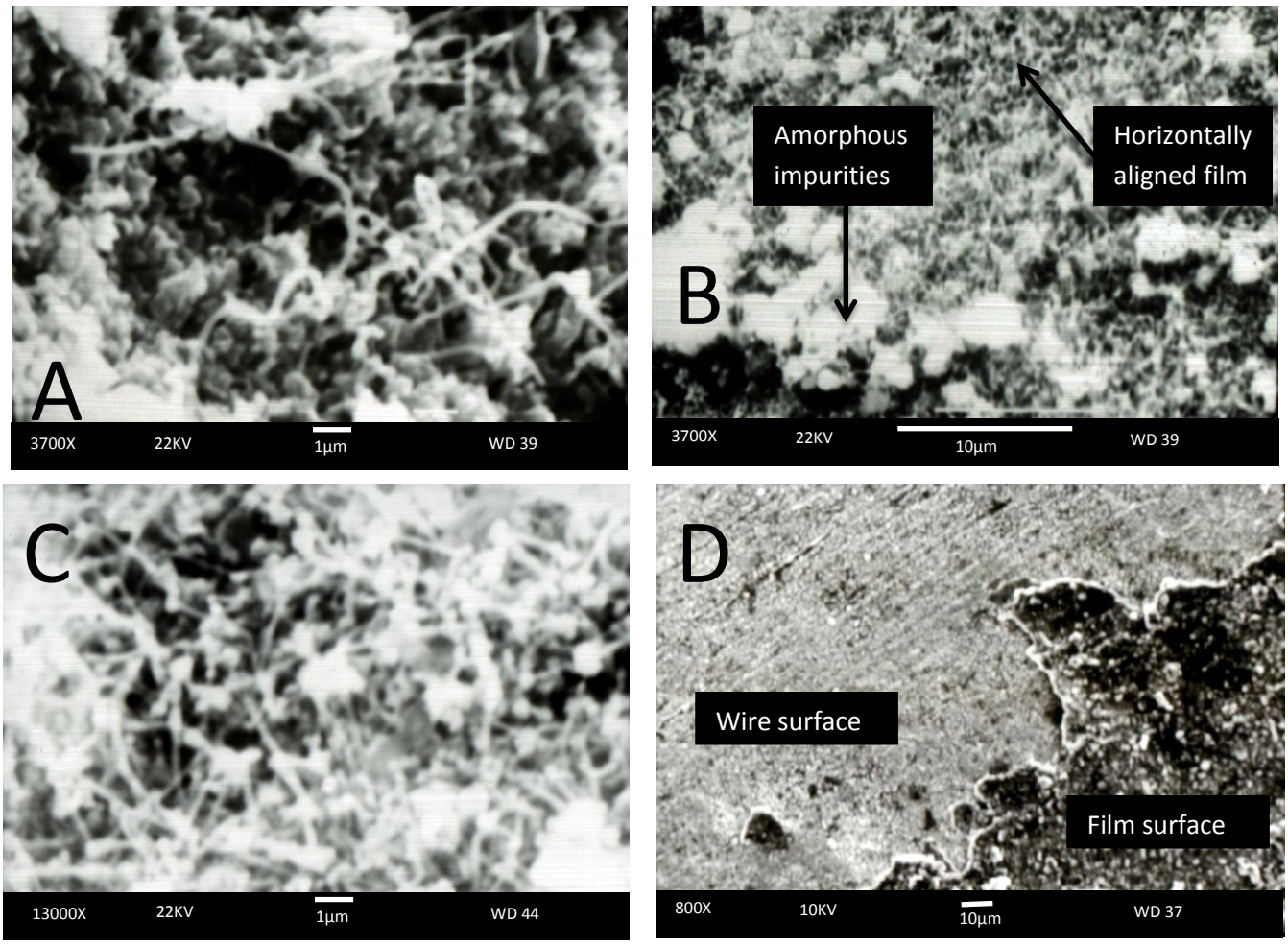

Figure 3.5: Carbonaceous film formed using pure acetylene process gas and ferrocene catalyst at 850^{o}C without catalyst pre-deposition, (A) impurities in the film prior to washing, (B) horizontally aligned nanotube film exposed through washing, (C) magnified image of nanotube film, (D) degradation of the film

argon gas at a flowrate of 647.3cm^3/min for a further 15 min. The reaction produced large carbon filaments ranging from 100 to 1500 nm as shown in Figure 3.6 A, as well as nanotubes and nanotube bundles as shown in Figure 3.6 B, C and D. The filaments were deposited on a nanotube film which is shown in Figure 3.6 D. the nanotubes form bundles due to the large, attractive van der Waals forces that occur between the smaller nanotubes [63] that can arrange themselves in parallel arrangement. The larger nanotubes are less flexible and do not form parallel arrangements as readily.

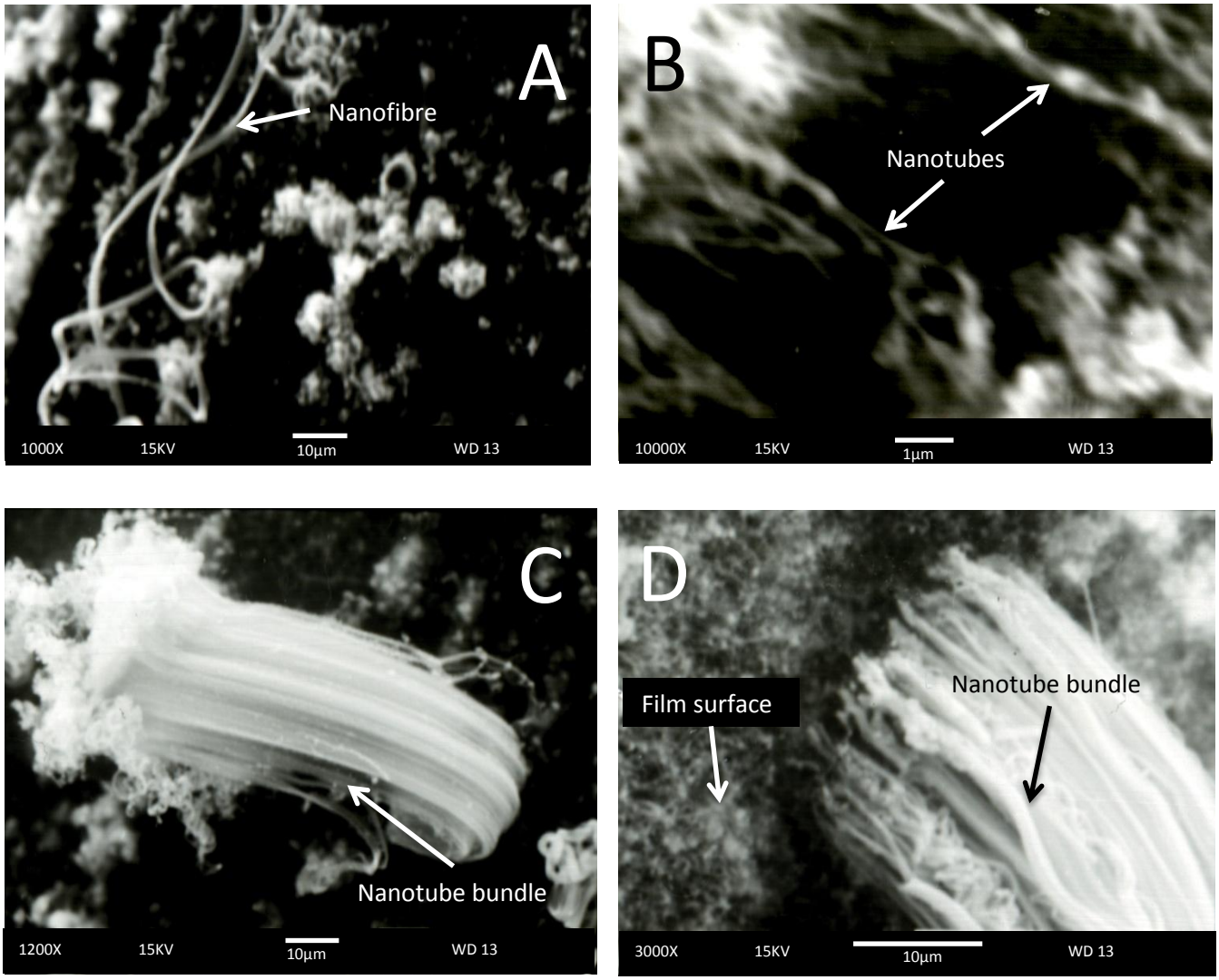

Figure 3.6: Carbonaceous film formed using pure acetylene process gas and ferrocene catalyst at 850^{o}C with catalyst pre-deposition, (A) nano-fibres on the film surface prior to washing, (B) nanotubes, approximately 100nm in diameter, on the film surface, (C) nanotube bundle on film surface, (D) nanotube bundle showing film surface

Washing the wires for 4 hours with distilled water removed the majority of the filaments and nanotube bundles, leaving the nanotube film mostly intact. Figure 3.7 A shows the nanotube film after washing, showing the presence of voids in the film that were not present prior to the washing procedure. The surface of the stainless steel can be seen in the void and is undamaged by the nanotube synthesis reaction. The film is formed from a densely packed layer of vertically aligned nanotubes and is approximately 20 µm thick, although the thickness of the film varied between 10 µm and 50 µm. as shown in Figure 3.7 B. The cause of the nanotube growth perpendicular to the surface of the wire as opposed to the

parallel deposition seen when nanotube synthesis was performed without catalyst pre-deposition is that during the catalyst pre-deposition stage the ferrocene catalyst is converted to the gaseous phase at 350^{o}C in the vaporiser and conveyed to the reactor by the argon gas. At 850^{o}C the ferrocene was decomposed to form iron particles that were deposited onto the surface of the wires which served as catalyst sites once the process gas was introduced into the reactor. In the case of synthesis without catalyst pre-deposition the ferrocene gas was conveyed from the reactor by the carbon containing process gas, thus as the ferrocene decomposed to form iron particles the particles immediately acted as the catalyst for the nanotube synthesis reaction and were deposited onto the surface of the wire once the nanotube was formed.

The vertically aligned nanotube film could act as a good carrier for cell immobilization as the film increases the surface area of the stainless steel wire through the formation of voids and fissures on the surface of the film as shown in Figure 3.8 A, this greatly increases the number of sites for cell immobilization and hence increases the maximum possible loading of cells on the nanotube film. Figure 3.8 A shows that some filaments remained on the surface of the film

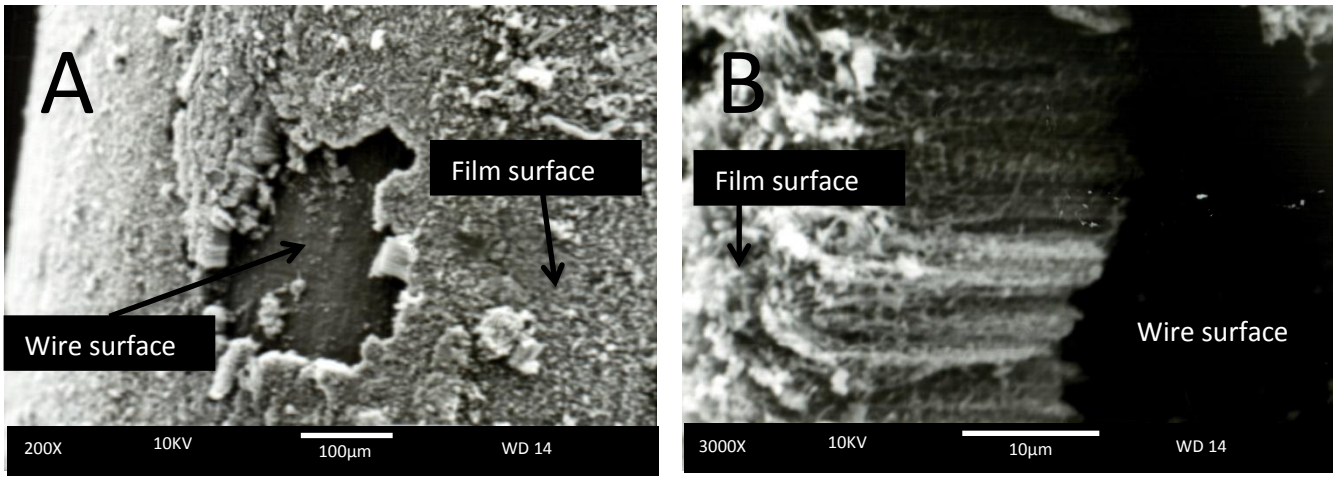

Figure 3.7: Carbonaceous film formed using acetylene and argon process gas and ferrocene catalyst at 850^{o}C with catalyst pre-deposition, (A) surface of nanotube film after washing with distilled water, (B) cross-sectional view of nanotube film after washing with distilled water

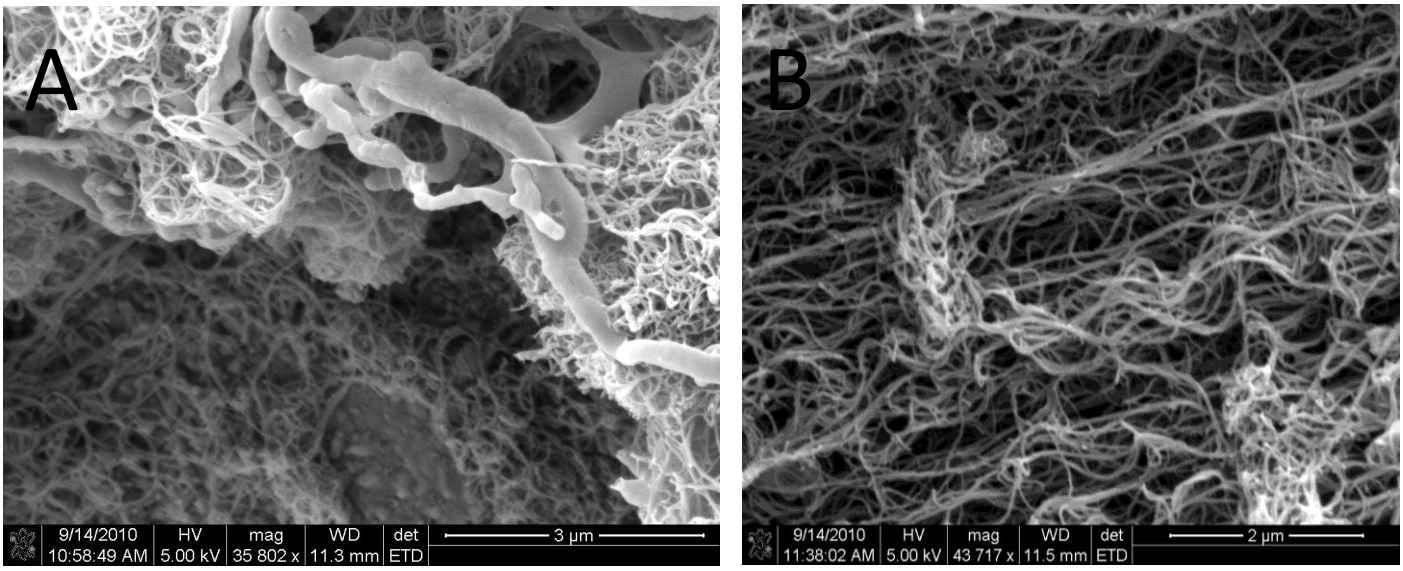

Figure 3.8: Carbonaceous film formed using acetylene and argon process gas and ferrocene catalyst at 850^{o}C with catalyst pre-deposition, (A) high magnification image of film showing nanotubes and fibres, (B) cross-sectional view of nanotube film after washing with distilled water

although the majority of the impurities were removed through washing with distilled water for 4 hours. The vertically aligned film is composed of nanotubes that range from 20 nm to 60 nm in diameter

3.3 Corrosion testing

The results of the corrosion testing are shown in Tables 3.1 and 3.2. Table 3.1 shows that the majority of the samples did not show signs of oxidation when immersed in distilled water for 24 hours, the exceptions being the stainless steel wires exposed to direct synthesis at 950^{o}C and the wires exposed to pre-deposition of catalyst without nanotube synthesis. The wires exposed to pre-deposition of catalyst followed by nanotube synthesis did not show any signs of oxidation. The wires exposed to pre-deposition of catalyst without subsequent nanotube synthesis showed visible signs of oxidation after immersion in distilled water however no other samples exposed to 850^{o}C showed any signs of oxidation. This shows that the oxidation is due to the deposition of iron particles rather than damage to the wire. The lack of visible oxidation on the wires after

nanotube synthesis shows that the catalyst particles are encapsulated by the carbon nanotubes preventing oxidation.

The wires exposed to nanotube synthesis at 950^{o}C showed damage to the surface as shown in Figure 3.2 D and Figure 3.3. The deposits shown in Figure 3.3 B correspond with the oxidation that was visible after 24 hour immersion in distilled water. As there was no addition of any metallic substance to the reactor in these cases the oxidation was caused from the sensitisation of the stainless steel. The high carbon concentration and high temperatures led to carbon diffusion into the steel, which reacted with the chromium in the surface of the steel to form carbides. This led to destruction of the oxide layer leading to the damage seen in the micrographs and the oxidation shown in Table 3.1.

Table 3.1: Results of tests performed on wire samples immersed in distilled water for 24 hours

Sample	**Catalyst**	**Reactor Temp (^{o}C)**	**Synthesis gasses**	**Formation of carbon filaments**	**Visible oxidation after 24 hr. immersion in distilled water**
1	none	600	acetylene	no	No
2	none	850	acetylene	Some filaments	No
3	none	950	acetylene	none	Yes
4	none	950	Acetylene, hydrogen	none	Yes
5	Ferrocene	850	acetylene	Horizontally aligned film	No
6	Ferrocene, pre-deposition	850	none	none	Yes
7	Ferrocene, pre-deposition	850	Acetylene, argon	Vertically aligned film	no

Table 3.2: weight loss due to immersion in 38% sulphuric acid for 24 hours

Wire sample	CNT coating	Mass Before (mg)	Mass After (mg)	Mass lost (mg)
Plain wire	No	129	126	3
Direct synthesis at 600^{o}C	No	150	143	7
Direct synthesis at 850^{o}C	No	135	126	9
Direct synthesis at 950^{o}C without H_2	No	163	160	3
Direct synthesis at 950^{o}C with H_2	No	155	151	4
Catalytic growth at 850^{o}C	Yes	140	140	0
Catalyst pre-deposition at 850^{o}C	Yes	135	134	1

The results of the sulphuric acid immersion tests, shown in Table 3.2, show that the samples without a coating of carbon nanotubes had significant mass loss. The samples that have a nanotube coating showed no significant mass loss over the 24 hour period. The equipment used to measure the mass of the wires is accurate to within 1 mg, hence a change in mass of more than 2 mg can be seen as significant. The total mass loss in the samples without the nanotube coating cannot however be assumed to be only corroded metal since the corrosion of the wire resulted in the carbon coating flaking off due to gas evolution on the surface on the metal during corrosion. In the case of the wires exposed to direct synthesis this coating is in the form of amorphous carbon, which is removed by acid treatment [(64)]. Since carbon nanotubes are not removed by acid treatment, the presence of the nanotube film provided protection from acidic corrosion for the 24 hour period. However the coating can be removed by hydrodynamic

forces, as shown in Figure 3.5 D, which would result in the loss of protection from acidic corrosion.

3.4 Immobilization of yeast cells on carbon nanotubes

The validity of using stainless steel coated with carbon nanotubes, produced through catalytic synthesis of carbon nanotubes were used as an immobilized cell carrier was examined by placing the coated wires in an actively fermenting medium containing a high concentration of free suspended yeast cells.

While the majority of the carbon nanotube film did not show any yeast cell immobilization, some yeast cells were found to adhere to the surface of both the nanotube film and the plain stainless steel, as shown in Figure 3.9 A and B. The yeast cells did however accumulate in some voids that were present in the film. Figure 3.9 C and D show cells that have accumulated in a void, however interactions between the cells and the nanotubes cannot be determined. Figure 3.9 C does show however that while there are many cells in the void, the surface of the nanotube film surrounding the void is devoid of cells. This seems to indicate that carbon nanotubes do not actively attract yeast cells as the cells in the void have accumulated due to the shelter from sheer forces that is provided by the vertically aligned nanotube film. Figure 3.9 D shows that the interactions between the cells are very strong and that some of the cells deeper in the void have become elongated.

Figure 3.10 A shows a cross sectional view of the vertically aligned carbon nanotube film showing no immobilized cells despite the sheltered area. Further examination of the surface of the film clearly showed the dense layer of carbon nanotubes, without any yeast cells present, as shown in Figure 3.10 B. The film

shows that while the surface area has increased due to the presence of nanotubes as stated by Gao et al. [22] the spaces between the nanotubes are far too small to allow penetration of cells. Hence the effective surface area for cell immobilization has not increased due to the presence of the nanotube film. This can be clearly seen in the yeast cells on the surface of the nanotube film shown in Figure 3.10 C and D. The high magnification images of the yeast cells on the surface of the nanotube film show the interaction between the cells and the nanotubes that comprise the film. The nanotubes appear to be flexible and

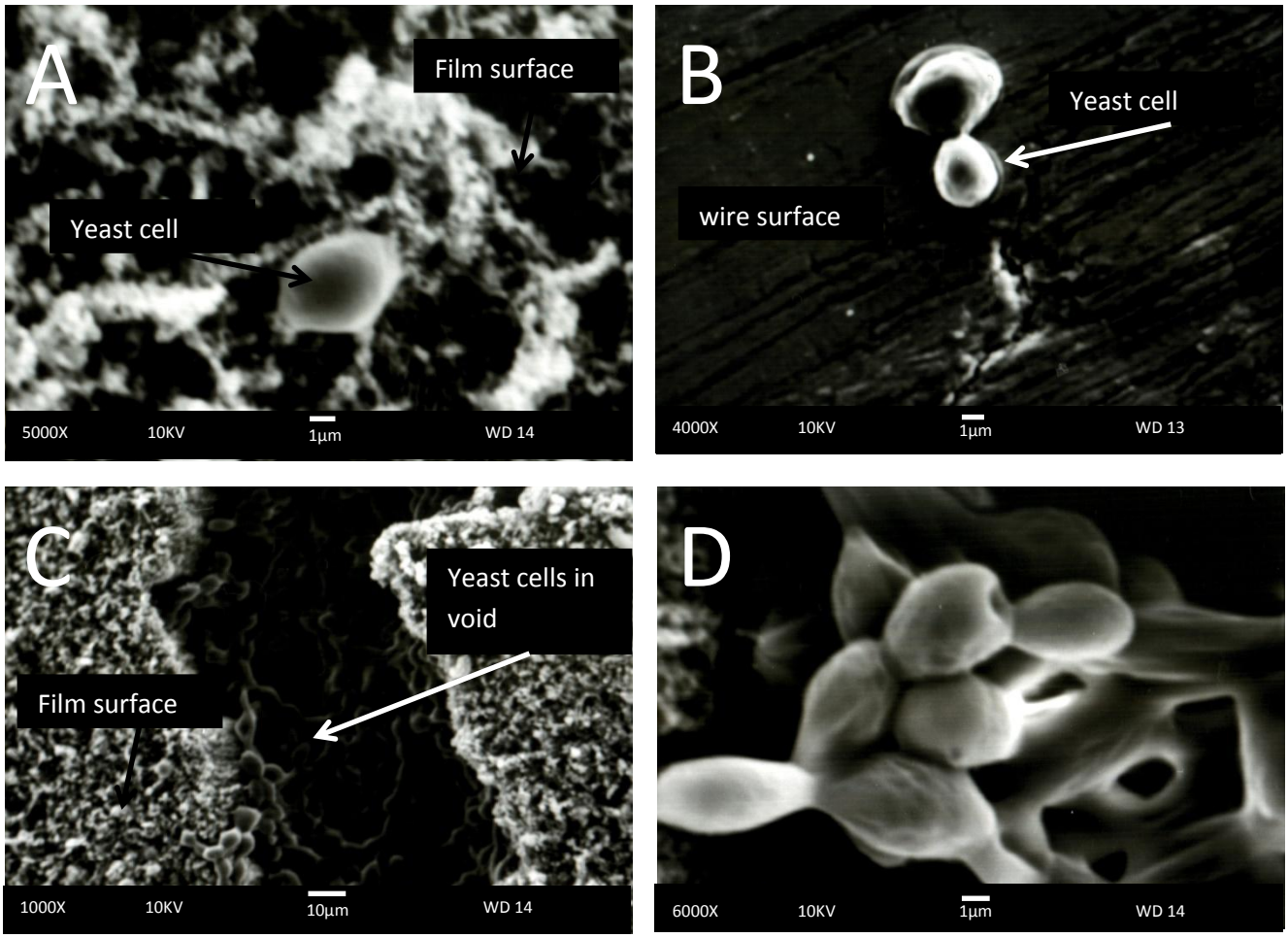

Figure 3.9: Yeast cells immobilized on stainless steel (A) CNT coated wire 2.7 hours after inoculation initial yeast concentration 1.94 g/l, (B) stainless steel without coating 39.5 hours after inoculation initial yeast concentration 0.57 g/l, (C) yeast cells accumulating in void 28.8 hours after inoculation initial yeast concentration 1.94 g/l, (D) magnified view of yeast cells in void

attach strongly to the cell wall of the yeast cells in a manner similar to that reported by Akasaka & Watari [56]. As the nanotubes that form the film are less than 50 nm in diameter, they retain the flexibility to wrap around the cell, providing for very strong attachment. The pores in the surface of the film may also indicate why so few cells attached to the film. The pores reduce the surface area in contact with the cells during the initial attachment, hence reducing the force holding the cell on the surface, hence most cells are washed out before adhesion can occur as found by Ju et al. [65].

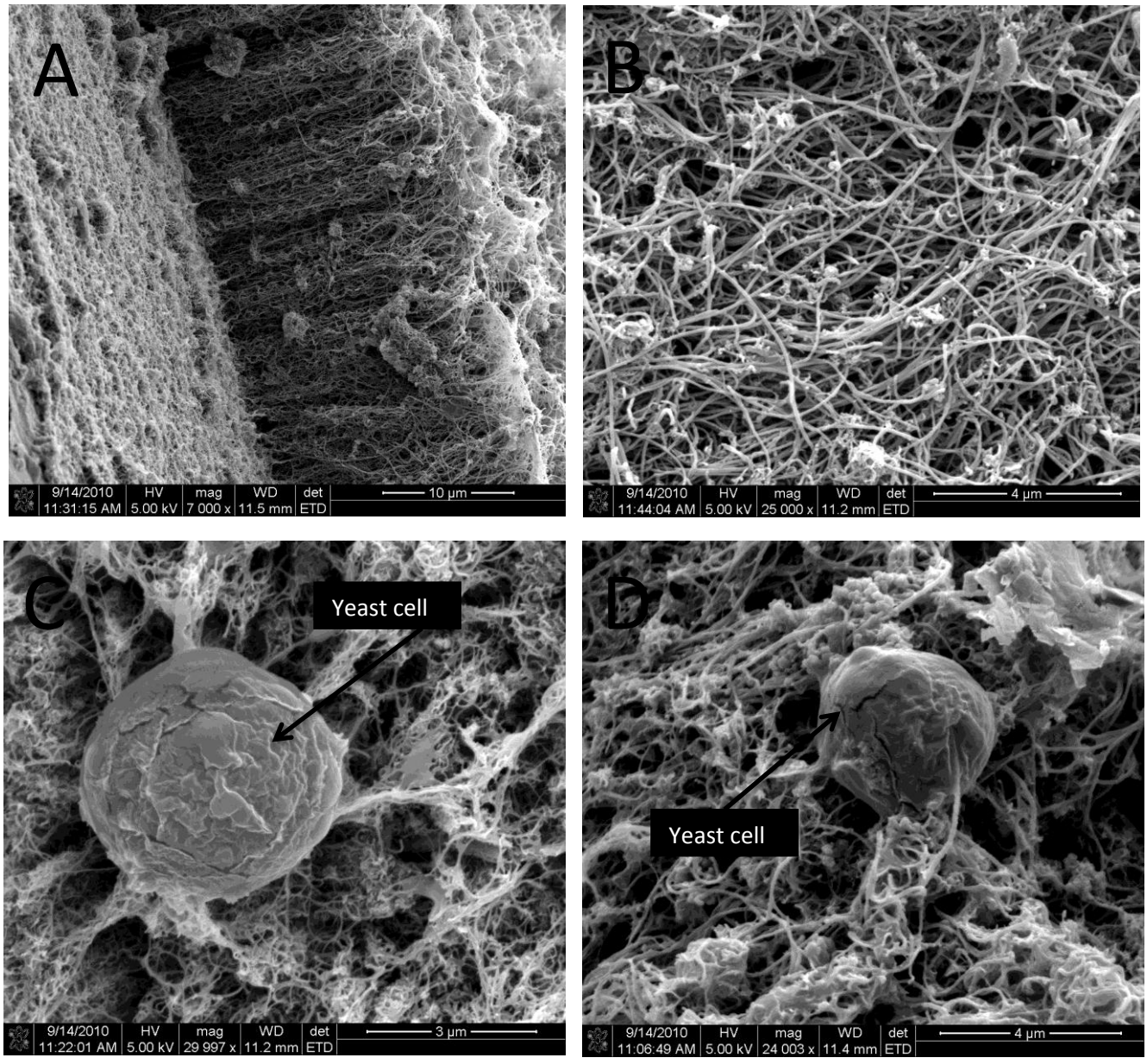

Figure 3.10: Carbon nanotube film after fermentation with initial yeast concentration 0.51 g/l: (A) large area of film with no yeast cells 9.7 hours after inoculation, (B) surface of CNT film 9.7 hours after inoculation, (C) & (D) yeast cells immobilized on CNTs 22.1 hours after inoculation

By comparison Figures 3.11 A and B show portions of the film that have been coated by an unidentified deposit preventing interactions between the cells and the nanotubes. In this case interactions between the cells and the surface do not seem to be very strong; however the cell-cell interactions seem to be very strong. The strength of cell-cell interactions can also be seen on the cells shown

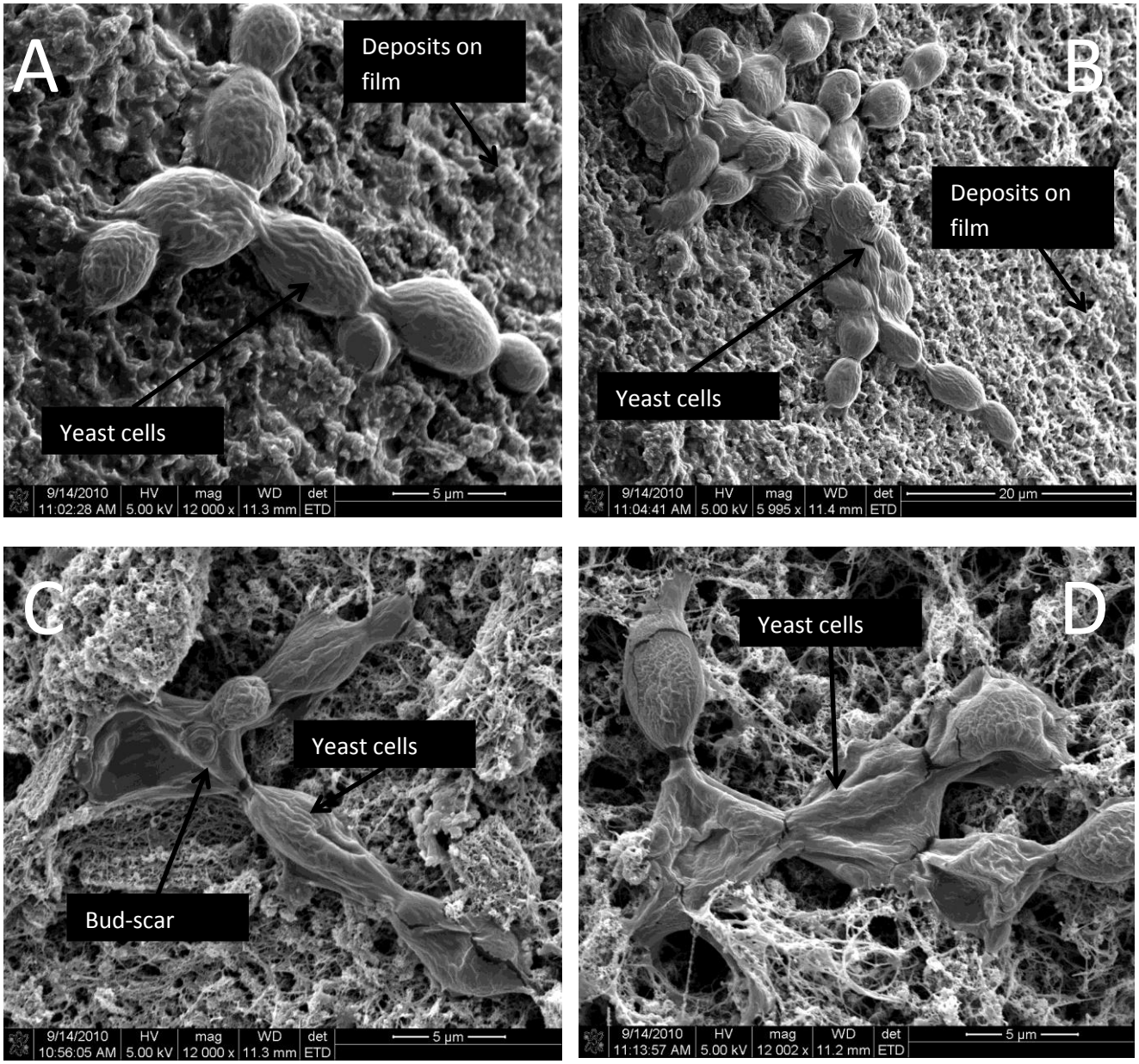

Figure 3.11: Immobilized yeast cell colonies after 22.1 hour fermentation initial yeast concentration 0.51 g/l (A) & (B) yeast immobilized on deposits, (C) & (D) yeast cells immobilized on CNTs

in Figures 3.11 C and D. In this case the cells are exposed to the nanotubes and the morphology of the cells has been completely changed by the presence of the nanotubes. The difference between the yeast cells shown in Figures 3.10 C and D and the cells in Figures 3.11 C and D is that the cells shown in Figures 3.11 C and D have obviously been attached to the nanotubes for a much longer time period as the cells have divided numerous times, leading to the formation of the cluster of cells seen on the nanotube film. The division of the cells also indicates that while the morphology of the cells has been radically altered due to the carbon nanotubes, the cells are still alive and multiplying. The change in morphology caused by the carbon nanotubes can be seen in Figures 3.12 A, B and C. The cells in the void, not attached to the carbon nanotubes retained a semi-ovoid shape, with minimal deformation. The cells that show contact with the carbon nanotubes became deformed, as they have been stretched by the forces exerted by the nanotubes. The cells also show evidence of cell division, and bud scars can be clearly seen on some of the highly deformed cells, indicating that the deformation of the cells does not necessarily mean that the cells have been killed.

Figures 3.12 A, B and C show cells that have been immobilized in a void in the film, hence both the shelter from shear forces and the interaction between the nanotubes and the cells leads to cell adhesion. In this case it can be seen that the cells that are not directly connected to the nanotubes, and are not deformed, benefit from the shelter from shear forces; however the strength of the cell-cell adhesion would probably prevent removal of the non-attached cells from the surface of the film. It is likely however that the presence of the void allows for the initial attachment of the cells leading to the strong adhesion seen in the micrographs. Most of the voids in the carbon nanotube film did not contain any cells however, as can be seen in Figure 3.12 D. The Figure shows cells immobilized on the surface of the film next to void containing no cells. The

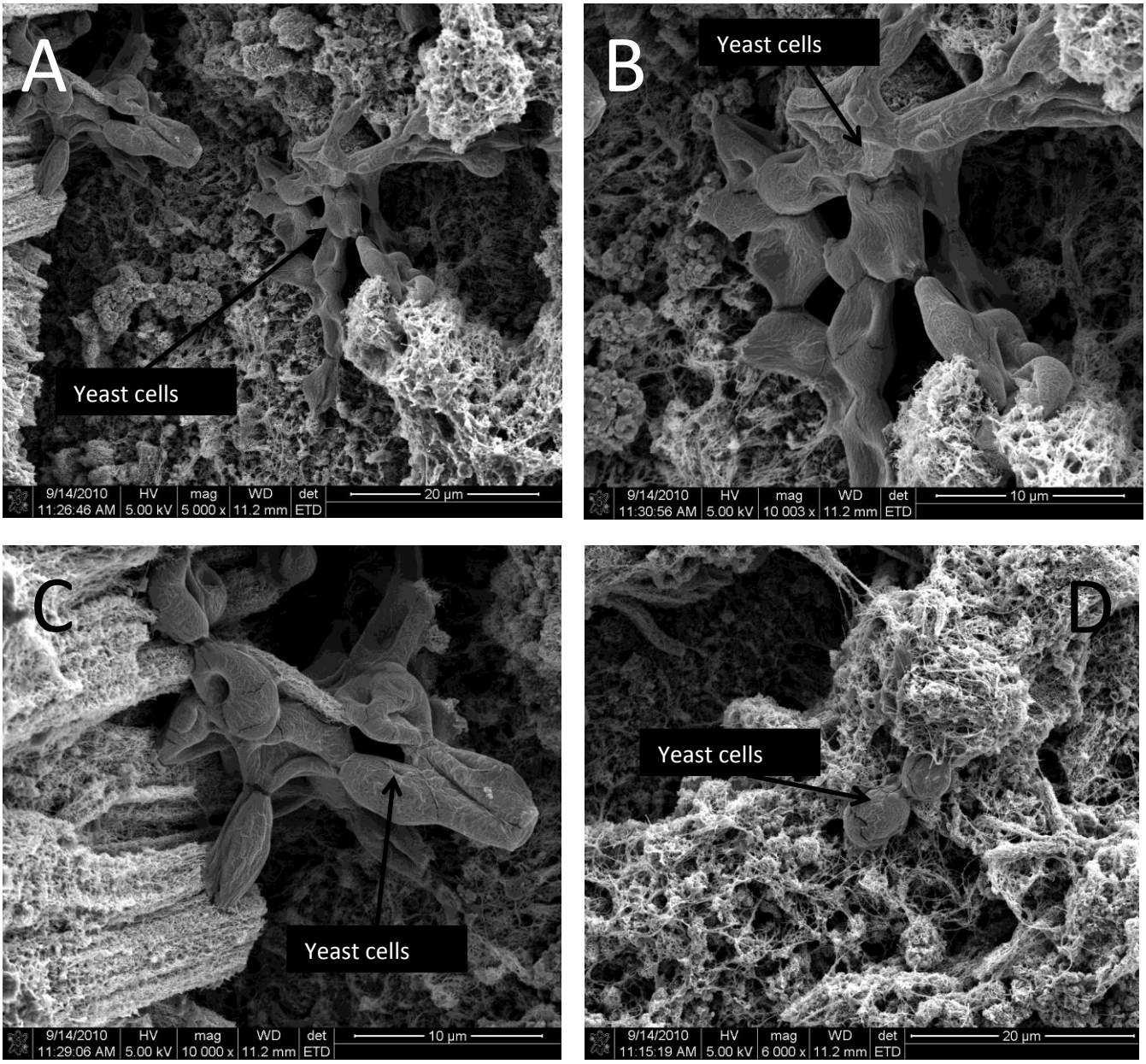

Figure 3.12: Yeast cells immobilized on CNTs, 22.1 hours after inoculation initial yeast concentration 0.51 g/l (A) yeast cells immobilized in void, (B) & (C) magnified view of yeast cells in void, (D) yeast cells immobilized on the film surface

formation of cell agglomerations in the voids is dependent on the initial cell entry into the void from the bulk solution. Once the cells enter a void they can become attached to the walls of the void as shown in Figure 3.12 A or the cells can attach to other yeast cells as shown in Figure 3.9 D.

While the majority of the deformed yeast cells showed signs of division and growth some cells were obviously dead, as shown in Figure 3.13 A. The cell in the micrograph has been damaged severely and the cell contents can be seen to have spilled out of the cell onto the carbon nanotube film. While this does not confirm the cytotoxicity of carbon nanotubes it does show that dead cells are retained by the film rather than being released. This does not allow for a reasonable biocatalyst material as the retention of dead cells would cause difficulties in regeneration of the biocatalyst. Further practical problems with using the carbon nanotube coated stainless steel wires as a biocatalyst support is the degradation of the film over time. Figure 3.13 B shows the break-down of the film with the pieces lying on the surface of the wire. The stability of the film is a very important aspect in terms of using a biocatalyst in food and beverage applications, as any break-down of the catalyst will result in the contamination of the product. The numerous voids that were found in the film also reflect the fragility of the film.

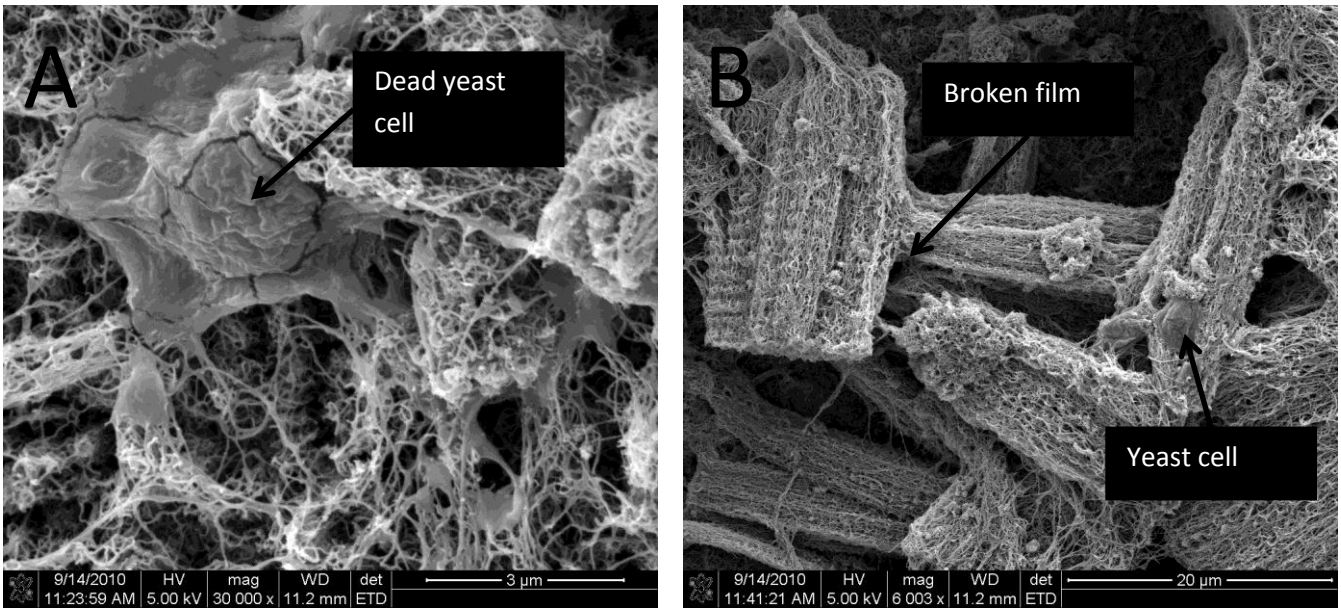

Figure 3.13: Carbon nanotube film 22.1 hours after inoculation initial yeast concentration 0.51 g/l (A) dead yeast cell, (B) broken film

The progression of the fermentations is shown in Figures 3.14 and 3.15. The concentration of yeast cells in suspension during the fermentations is shown in Figure 3.14, and shows the comparison of the data to the logistic curve growth model given as Equation 4. The logistic curve model was fitted to each data set using a least squares regression of the data during the exponential and stationary growth phases of the yeast. Figure 3.14 shows that the yeast did not show any noticeable growth for the first 9.7 hours after inoculation. The initial lag phase was followed by a long exponential growth phase, a short stationary phase and finally flocculation. The concentration of yeast cells in suspension decreased rapidly for all fermentations after the maximum yeast cell concentration was achieved. This shows that the strain of yeast that was used was highly flocculent. Samples taken during the various growth stages showed no noticeable increase in the number of immobilized cells during any phase. However the samples taken during and after the exponential growth phase show more groups of cells as seen in Figure 11, C and D. Thus it can be concluded that the groups of cells are formed through cell division of immobilized cells rather than entrapment of cells from the bulk fluid. This shows that the immobilization of cells is not reversible as the cells remain immobilized through several replications.

The maximum yeast cell concentration in suspension, X_m, did not depend on the initial cell concentration, X_0, as the highest and lowest initial yeast concentrations resulted in X_m values of 4.415 g/l and 4.444 g/l respectively. Figure 3.15 shows that the higher initial yeast concentration resulted in a faster rate of ethanol production. However the total ethanol produced ranged between 28.16 g/l and 29.01 g/l By comparing the biomass yield, Y_X, shown in Table 3.3, it can be seen that the biomass yield for the highest initial yeast concentration was only 64% of that for the lowest initial yeast concentration. However the ethanol yield, Y_P, for the fermentation using the highest initial yeast concentration was

only 3.1% higher than that of the lowest initial yeast concentration. Thus it would be expected for the highest initial yeast concentration to attain a much higher biomass yield and consequently a higher maximum yeast cell concentration. However, due to the flocculent nature of the yeast, excess yeast flocculated once the maximum yeast concentration was reached. This is also shown by the longer stationary phase experienced by the fermentation using the highest initial concentration of yeast, which lasted from 25.8 hours until flocculation occurred at 34.3 hours, by contrast the lowest initial concentration of yeast experienced a stationary phase from 34.3 hours until flocculation at 39.5 hours. The longer stationary phase should have resulted in much higher ethanol production, thus a

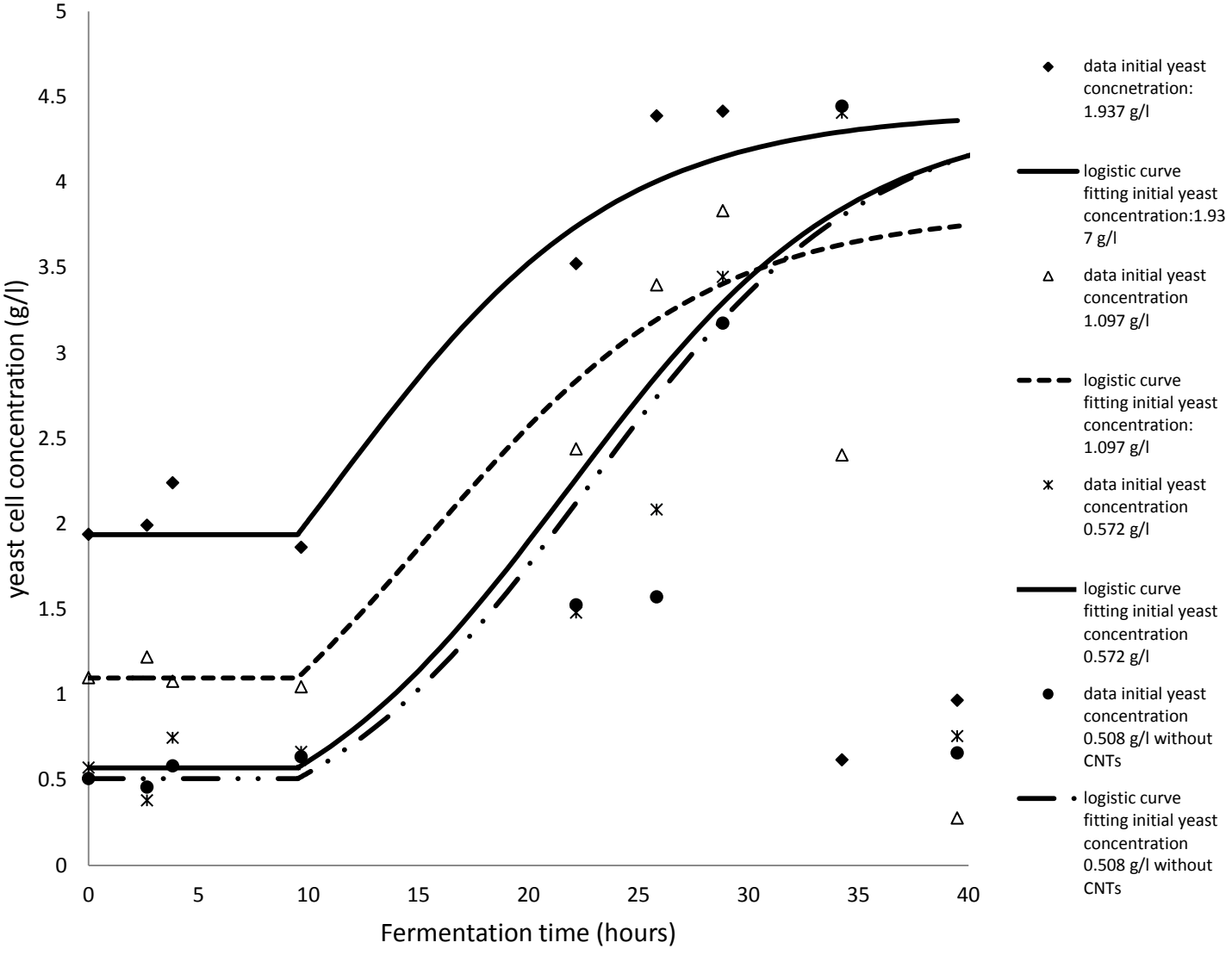

Figure 3.14: Yeast concentration in bulk fluid during fermentation showing logistic curve fitting

higher ethanol yield. However the yeast continued to grow aerobically during the stationary phase and the excess yeast flocculated out of suspension and thus was not measured in the bulk fluid.

The aerobic nature of the fermentation can be seen by examining the ethanol yields of the fermentations. The fermentations only achieved between 61% and 64% of the theoretical maximum yield of 0.511 g of ethanol per g carbohydrate. This indicates that mixing resulted in aeration of the fermentation media, as the flasks were not closed to the atmosphere.

The effect of the immobilization of yeast cells on the growth and fermentation kinetics could not be adequately determined due to the low number of yeast

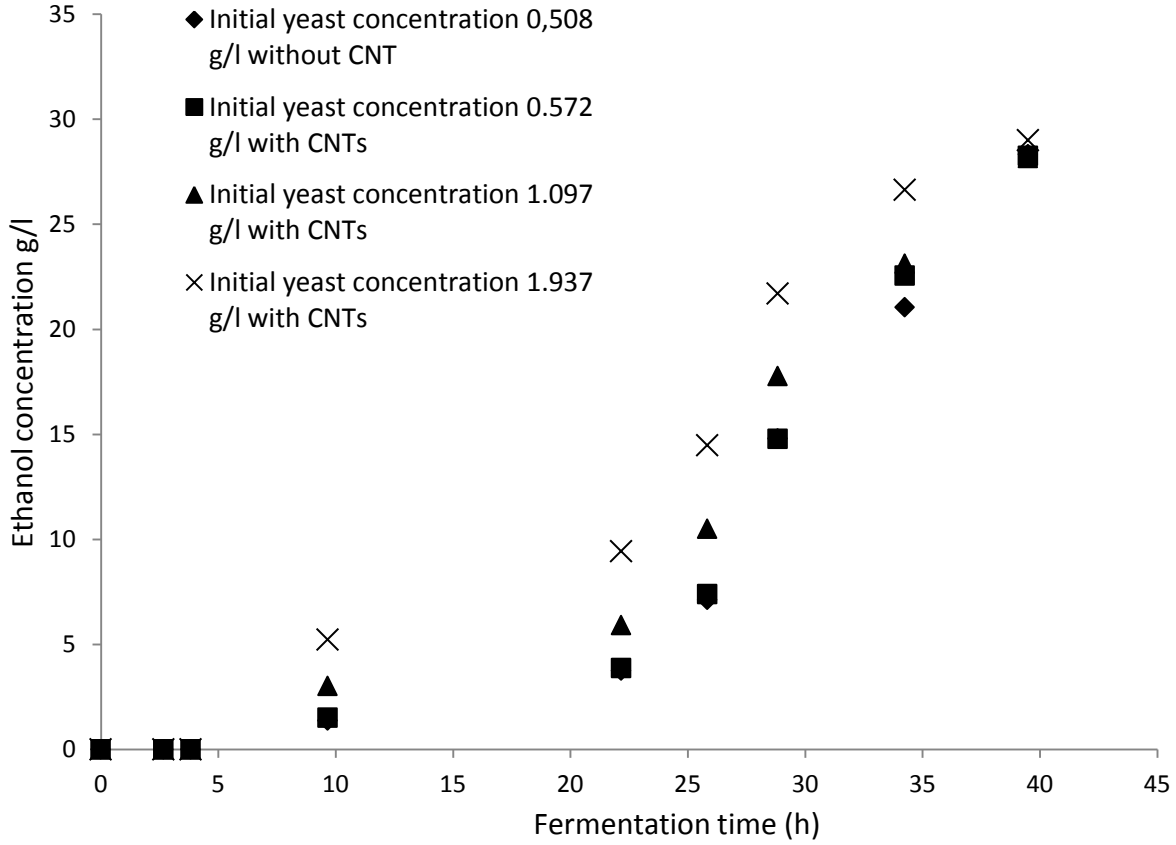

Figure 3.15: Ethanol concentration increase during fermentation

cells that were immobilized. In each case, less than 1% of the surface of the film was covered with yeast cells; hence each 10 cm length of wire retained less than 0.035 mg of immobilized yeast. Thus 22.1 hours after inoculation with an initial yeast concentration of 0.51 g/l; less than 0.01% of the yeast present in the fermentation was immobilized on the wire, and hence had a negligible effect on the growth and fermentation of the yeast in suspension. The fermentations using similar initial yeast concentrations, with and without CNTs present, did not differ greatly as the fermentation containing the CNT coated wire, using an initial yeast concentration of 0.572 g/*l*, resulted in a maximum yeast concentration of 4.405 g/*l* and a final ethanol concentration of 28.264 g/*l.* The fermentation containing the stainless steel wire without the CNT coating, using an initial yeast concentration of 0.508, attained a maximum yeast concentration of 4.444 g/*l* and a final ethanol concentration of 28.342 g/*l*.

Table 3.3: Data obtained from fermentations

	Initial yeast concentration: 0.508 g/l without CNTs	Initial yeast concentration: 0.572 g/l	Initial yeast concentration 1.097 g/l	Initial yeast concentration 1.937 g/l
X_m (g/l)	4.444	4.405	3.832	4.415
μ h^{-1}	0.155	0.166	0.184	0.251
S_0 (g/l)	93.047	93.778	92.029	92.862
S_{final} (g/l)	3.281	3.201	3.166	3.918
Etoh (g/l)	28.342	28.264	28.159	29.010
Y_p (g/g)	0.315	0.313	0.317	0.326
Y_x (g/g)	0.044	0.049	0.031	0.028

The feasibility of the use of the CNT film during fermentation is however, limited due to the low coverage of immobilized cells. If 100% coverage was achieved the biocatalyst would have a loading of approximately 12.56 g yeast/m^2, however as the coverage was less than 1% this drops to less than 0.13 g/m^2. This means to have 1 g of yeast cells immobilized on the wires used in these experiments would require over 2.8 km of wire. Thus to have an inoculation of 3 g of yeast per litre of wort, would require each ml of wort to be in contact with over 0.024 m^2 of biocatalyst. To achieve such a contact ratio the bulk solution would be a film that is less than 41.88 µm thick, which is not feasible. Many other carriers have been used successfully for fermentation. For example Yu et al. (2010) [65] achieved yeast loading on modified sorghum bagasse which was sufficient for ethanol production, and the carrier did not degrade in 20 days of continuous fermentation. The degradation of the CNT film renders the use of such a film for beer fermentation inadequate. Aside from contamination of the product, the degradation would render the biocatalyst inoperable, hence the biocatalyst does not satisfy the conditions required for beverage production given in section 1.4.5.

4 Conclusions and recommendations

4.1 Production of carbon nanotubes on stainless steel

The results showed that the most effective method to produce a carbon nanotube film on stainless steel, for the purpose of cell immobilization was the use of catalyst pre-deposition, followed by nanotube synthesis using acetylene with argon as a carrier gas at 850^{o}C. The film was found to comprise two distinct layers. The top layer was comprised of nanotube bundles and large carbon filaments, which were deposited on top of a layer of vertically aligned nanotubes formed perpendicular to the surface of the stainless steel. It was found that the nanotube bundles and large filaments were removed via washing in distilled water, while the vertically aligned nanotubes remained as a stable film, although some voids and fissures were formed in the film due to the washing process. The film is adequate for use in cell immobilization due to the stability in liquid media as well as the increased surface area that the film provides. The film was shown to be stable in distilled water for 4 hours; however exposure to various stresses such as shear forces and handling during the fermentation experiments lead to the degradation of the film, which leads to the conclusion that a carbon nanotube film produced via the method described earlier is not adequate for use in beer brewing, or for any beverage application due to possible contamination of the final product.

4.2 Immobilization of yeast cells on carbon nanotubes for beer production

The use of carbon nanotubes as an immobilized cell carrier for beer production is not feasible due to the low coverage rates achieved. The hypothesis that the biocatalyst would provide adequate fermentation kinetics for beer fermentation

was disproved due to the incredibly large surface area of biocatalyst that would be required to attain a useful yeast concentration. Carbon nanotubes were shown to interact strongly with the yeast cells in short range adhesion, but did not seem to have an effect on the long range forces affecting the initial attachment of yeast cells to the carbon nanotubes. The strength of the short range adhesion is also problematic for the use of the CNT film as a biocatalyst as regeneration of the biocatalyst would be complicated by the retention of dead cells on the surface of the film.

4.3 Recommendations

There is a possibility that a film of carbon nanotubes could be used as the site for cell adsorption but the lack of long range attraction between the yeast cells and the carbon nanotubes, at beer fermentation conditions, indicates that the film is not useful for yeast cell adsorption for beer brewing. The strong short range interaction between the yeast cells and the carbon nanotubes however indicate that a carbon nanotube film could provide an excellent substrate for cell growth where formation of a biofilm is required. Thus applications such as biomedical scaffolding and waste water treatment could use cells immobilized on carbon nanotubes.

References

1. Iijima, S.; others. Helical microtubules of graphitic carbon. *nature* **1991,** *354* (6348), 56-58.

2. Fitzer, E.; Kochling, K.; Boehm, H.; Marsh, H. Recommended terminology for the discription of carbon black as a solid (IUPAC recommendations 1995). *Pure and Applied Chemistry* **1995,** *67,* 573-506.

3. Liu, Z.; Chen, K.; Davis, C.; Sherlock, S.; Cao, Q.; Chen, X.; Dai, H. Drug Delivery with Carbon Nanotubes for In vivo Cancer Treatment. *Cancer Research* **2008,** *68,* 6652.

4. Lee, Y. B.; Lee, C. H.; Lim, D. S. The electrical and corrosion properties of carbon nanotube coated 304 stainless steel/polymer composite as PEM fuel cell bipolar plates. *International Journal of Hydrogen Energy* **2009,** *34* (24), 9781-9787.

5. Sotiropoulou, S.; Chaniotakis, N. Carbon nanotube array-based biosensor. *Analytical and Bioanalytical Chemistry* **2003,** *375,* 103-105.

6. Correa-Duarte, M.; Wagner, N.; Rojas-Chapana, J.; Morsczeck, C.; Thie, M.; Giersig, M. Fabrication and biocompatability of carbon nanotube based 3D networks as scaffolds for cell seeding and growth. *Nano Letters* **2004,** *4,* 2233-2236.

7. Upadhyayula, V. K. K.; Deng, S.; Smith, G. B.; Mitchell, M. C. Adsorption of *Bacillus subtilis* on single-walled carbon nanotube aggregates, activated carbon and NanoCeram (TM). *Water Research* **2009,** *43* (1), 148-156.

8. Jos; Miki-Yoshida, M.; Rendon, L.; Santiesteban, J. Catalytic growth of carbon microtubules with fullerene structure. *Applied physics letters* **1993,** *62,* 657.

9. Sinnott, S.; Andrews, R.; Qian, D.; Rao, A.; Mao, Z.; Dickey, E.; Derbyshire, F. Model of carbon nanotube growth through chemical vapor deposition. *Chemical Physics Letters* **1999,** *315* (1-2), 25-30.

10. Dupuis, A. The catlyst in the CCVD of carbon nanotubes. *Progress in Materials Science* **2005,** *50,* 929-961.

11. Baker, R.; Harris, P.; Thomas, R.; Waite, R. Formation of filamentous carbon from iron, cobalt and chromium catalyzed decomposition of acetylene. *Journal of Catalysis* **1973,** *30* (1), 86-95.

12. Pirard, S.; Heyen, G.; Pirard, J. Quantitative study of catalytic activity and catalytic deactivation of Fe-Co/Al2O3 catalysts for multi-walled carbon nanotube synthesis by the ccvd process. *Applied Catalysis A: General* **2010,** *382,* 1-9.

13. Lee, Y. T.; Kim, N. S.; Park, J.; Han, J. B.; Choi, Y. S.; Ryu, H.; Lee, H. J. Temperature dependent growth of carbon nanotubes by pyrolysis of ferrocene and acetylene in the range between 700 and 1000 C. *Chemical Physics Letters* **2003,** *372,* 853-859.

14. Bai, S.; Yang, Q.; Chen, H.; Bai, J. Influence of ferrocene/benzene mole ratio on the synthesis of carbon nanostructures. *Chemical Physics Letters* **2003,** *376,* 83-89.

15. Afolabi, A. S.; Abdulkareem, A. S.; Iyuke, S. E. Synthesis of carbon nanotubes and nanoballs by swirled floating catalyst chemical vapour deposition methof. *Journal of Experimental Nanoscience* **2007,** *2,* 269-277.

16. Kuwana, K.; Saito, K. Modeling ferrocene reactions and iron nanoparticle formation: Application to CVD synthesis of CArbon nanotubes. *Proceedings of the Combustion Institute* **2007,** *31,* 1857-1864.

17. Van der Wal, R.; Ticich, T.; Curtis, V. Diffusion flame synthesis of single walled carbon nanotubes. *Chemical Physics Letters* **2000,** *323,* 217-223.

18. Van der Wal, R.; Hall, L. J. Carbon nanotube synthesis upon stainless steel meshes. *Carbon* **2003,** *41* (4), 659-672.

19. Murphy, D.; Carroll, R. Kinetics and mechanism of carbon film deposition by acetylene pyrolysis. *Carbon* **1992,** *30,* 47-54.

20. Neumayer, H.; Haubner, R. Formation of carbon nano-fibres and carbon-nanotubes with a vertical flow-reactor. *Diamond and Related Materials* **2004,** *13,* 1191-1197.

21. Cho, J.; Konopka, K.; Rozniatowski, K.; Garc; Shaffer, M. S. P.; Boccaccini, A. R. Characterisation of carbon nanotube films deposited by electrophoretic deposition. *Carbon* **2009,** *47* (1), 58-67.

22. Gao, L.; Kiwi-Minsker, L.; Renken, A. Growth of carbon nanotubes and microfibers over stainless steel mesh by cracking of methane. *Surface and Coatings Technology* **2008,** *202* (13), 3029-3042.

23. Nerushev, O. A.; Sveningsson, M.; Falk, L. K. L.; Rohmund, F. Carbon nanotube films obtained by thermal chemical vapour deposition. *Journal of Materials Chemistry* **2001,** *11* (4), 1122-1132.

24. Abad, M.; S; Berenguer-Murcia, A.; Golovko, V.; Cantoro, M.; Wheatley, A.; Fern; Johnson, B.; Robertson, J. Catalytic growth of carbon nanotubes on stainless steel: Characterization and frictional properties. *Diamond and Related Materials* **2008,** *17* (11), 1853-1857.

25. Karwa, M.; Iqbal, Z.; Mitra, S. Scaled-up self-assembly of carbon nanotubes inside long stainless steel tubing. *Carbon* **2006,** *44* (7), 1235-1242.

26. Yuan, L.; Saito, K.; Hu, W.; Chen, Z. Ethylene flame synthesis of well-aligned multi-walled carbon nanotubes. *Chemical physics letters* **2001,** *346* (1-2), 23-28.

27. Martínez-Hansen, V.; Latorre, N.; Royo, C.; Romeo, E.; García-Bordejé, E.; Monzón, A. Development of aligned carbon nanotubes layers over stainless steel mesh monoliths. *Catalysis Today* **2009,** *147* (Supplement 1), S71 - S75, 3rd International Conference on Structured Catalysts and Reactors, ICOSCAR-3, Ischia, Italy, 27-30 September 2009.

28. Park, D.; Kim, Y. H.; Lee, J. K. Pretreatment of stainless steel substrate surface for the growth of carbon nanotubes by PECVD. *Journal of Materials Science* **2003,** *38* (24), 4933-4939.

29. Baddour, C. E.; Fadlallah, F.; Nasuhoglu, D.; Mitra, R.; Vandsburger, L.; Meunier, J. L. A simple thermal CVD method for carbon nanotube synthesis on stainless steel 304 without the addition of an external catalyst. *Carbon* **2009,** *47* (1), 313-318.

30. Masarapu, C.; Wei, B. Direct growth of aligned multiwalled carbon nanotubes on treated stainless steel substrates. *Langmuir* **2007,** *23* (17), 9046-9049.

31. Kaewsai, D.; Singjai, P.; Watcharapasorn, A.; Niranartlumpong, P. Growth of CNTs on Stainless Steel Particles. *Journal of Microscopy Society of Thailand* **2009,** *23(1),* 123-126.

32. Park, S. J.; Lee, D. G. Development of CNT-metal-filters by direct growth of carbon nanotubes. *Current Applied Physics* **2006,** *6,* e182--e186.

33. Baer, D. R. Protective and Non-Protective Oxide formation on 304 Stainless Steel. *Aplications of Surface Science* **1981,** *7,* 69-82.

34. Chu, F. W.; Rahmel, A. Conversion of Chromium Oxide to Chromium Carbide. *Oxidation of Metals* **1981,** *15,* 331-337.

35. Smith, G. M.; Young, D. J.; Trimm, D. L. Carburization Kinetics of Heat-Resistant Steels. *Oxidation of Metals* **1982,** *18,* 229-243.

36. Blair, M. G.; Pigman, W. Factors affecting the yield of alcohol in the fermentation of-glucose. *Archives of Biochemistry and Biophysics* **1953,** *42* (2), 278-292.

37. Bering, C. L. The Biochemistry of Brewing. *Journal of Chemical Education* **1988,** *65* (6), 519-530.

38. Fraleigh, S.; Bungay, H.; Fiechter, A. Regulation of oxidoreductive yeast metabolism by extracellular factors. *Journal of Biotechnology* **1989,** *12* (3-4), 185-198.

39. Bai, F.; Anderson, W.; Moo-Young, M. Ethanol fermentation technologies from sugar and starch feedstocks. *Biotechnology advances* **2008,** *26* (1), 89-105.

40. Kourkoutas, Y.; Bekatorou, A.; Banat, I.; Marchant, R.; Koutinas, A. Immobilization technologies and support materials suitable in alcohol beverages production: a review. *Food Microbiology* **2004,** *21* (4), 377-397.

41. Freeman, A. Gel entrapment of whole cells in cross-linked prepolymerized polyacrylamide-hydrazide gels. *Methods in Enzymology* **1987,** *135,* 216-222.

42. Martin, A. M., Ed. *Bioconversion of waste materials to industrial products;* Elsevier Apllied Science: New York, 1991.

43. Willaert, R.; Nedovic, V. A. Primary beer fermentation by immobilised yeast-a review on flavour formation and control strategies. *Journal of Chemical Technology \& Biotechnology* **2006,** *81* (8), 1353-1367.

44. Bezbradica, D.; Obradovic, B.; Leskosek-Cukalovic, I.; Bugarski, B.; Nedovic, V. Immobilization of yeast cells in PVA particles for beer fermentation. *Process Biochemistry* **2007,** *42* (9), 1348-1351.

45. Bekers, M.; Ventina, E.; Karsakevich, A.; Vina, I.; Rapoport, A.; Upite, D.; Kaminska, E.; Linde, R. Attachment of yeast to modified stainless steel wire spheres, growth of cells and ethanol production. *Process Biochemistry* **1999,** *35* (5), 523-530.

46. Plessas, S.; Bekatorou, A.; Koutinas, A.; Soupioni, M.; Banat, I.; Marchant, R. Use of *Saccharomyces cerevisiae* cells immobilized on orange peel as biocatalyst for alcoholic fermentation. *Bioresource technology* **2007,** *98* (4), 860-865.

47. Dragone, G.; Mussatto, S. I.; Silva, J. B. A. e. High gravity brewing by continuous process using immobilised yeast: effect of wort original gravity on fermentation performance. *Journal of the Institute of Brewing* **2007,** *113* (4), 391-398.

48. Reddy, V. L.; Reddy, K. H.; Reddy, P. L.; Reddy, V. O. Wine production by novel yeast biocatalyst prepared by immobilization on watermelon (Citrullus vulgaris) rind pieces and characterization of volatile compounds. *Process Biochemistry* **2008,** *43,* 748-752.

49. Yu, J.; Zhang, X.; Tan, T. A novel immobilization method of *Saccharomyces cerevisiae* to sorghum bagasse for ethanol production. *Journal of biotechnology* **2007,** *129* (3), 415-420.

50. Birol, G.; Doruker, P.; Kirdar, B.; Onsan, Z.; Ulgen, K. Mathematical description of ethanol fermentation by immobilised Saccharomyces cerevisiae. *Process Biochemistry* **1998,** *7,* 763-771.

51. Mitchell, D.; von Meien, O.; Krieger, N.; Dalsenter, F. A review of recent developments in modeling of microbial growth kinetics and intraparticle phenomena in solid-state fermentation. *Biochemical Engineering Journal* **2004,** *17,* 15-26.

52. Loosdrecht, M. C. M. v.; Lyklema, J.; Norde, W.; Zehnder, A. J. B. Bacterial adhesion: a physicochemical approach. *Microbial Ecology* **1989,** *17* (1), 1-15.

53. Br; Vicente, A.; Oliveira, R.; Teixeira, J. Physicochemical surface properties of brewing yeast influencing their immobilization onto spent grains in a continuous reactor. *Biotechnology and bioengineering* **2004,** *88* (1), 84-93.

54. Klein, J.; Ziehr, H. Immobilization of microbial cells by adsorption. *Journal of biotechnology* **1990,** *16* (1-2), 1-15.

55. Wang, H.; Gu, L.; Lin, Y.; Lu, F.; Meziani, M. J.; Luo, P. G.; Wang, W.; Cao, L.; Sun, Y. P. Unique aggregation of anthrax (*Bacillus anthracis*) spores by sugar-coated single-walled carbon nanotubes. *J. Am. Chem. Soc* **2006,** *128* (41), 13364-13365.

56. Akasaka, T.; Watari, F. Capture of bacteria by flexible carbon nanotubes. *Acta Biomaterialia* **2009,** *5,* 607-612.

57. Hu, H.; Ni, Y.; Montana, V.; Haddon, R.; Parpura, V. Chemically functionalized carbon nanotubes as substrates for neuronalo growth. *Nano Letters* **2004,** *4,* 507-511.

58. Zanello, L.; Zhao, B.; Hu, H.; Haddon, R. Bone cell proliferation on carbon nanotubes. *Nano Letters* **2006,** *6,* 562-567.

59. Lam, C. W.; James, J. T.; McCluskey, R.; Hunter, R. L. Pulmonary toxicity of single-wall carbon nanotubes in mice 7 and 90 days after intratracheal instillation. *Toxicological Sciences* **2004,** *77* (1), 126.

60. Warheit, D. B.; Laurence, B.; Reed, K. L.; Roach, D.; Reynolds, G.; Webb, T. Comparative pulmonary toxicity assessment of single-wall carbon nanotubes in rats. *Toxicological Sciences* **2004,** *77* (1), 117.

61. Kang, S.; Pinault, M.; Pfefferle, L. D.; Elimelech, M. Single-walled carbon nanotubes exhibit strong antimicrobial activity. *Langmuir* **2007,** *23* (17), 8670-8673.

62. Jia, G.; Wang, H.; Yan, L.; Wang, X.; Pei, R.; Yan, T.; Zhao, Y.; Guo, X. Cytotoxicity of carbon nanomaterials: single-wall nanotube, multi-wall nanotube, and fullerene.

Environ. Sci. Technol **2005,** *39* (5), 1378-1383.

63. Zhu, C.; Xie, Z.; Guo, K. Formation of close packed multi-walled carbon nanotube bundles. *Diamond and Related Materials* **2004,** *13,* 180-183.

64. Yu, X.; Lin, B.; Gong, B.; Jin, J.; Wang, R.; Wei, K. Effect of nitric acid treatment on carbon nanotubes (CNTs)-cordierite monoliths supported by ruthenium catalysts for ammonia synthesis. *Catalysis Letters* **2008,** *124,* 168-173.

65. Yu, J.; Yue, J.; Zhong, J.; Zhang, X.; Tan, T. Immobilization of *Saccharomyces cerevisiae* to modified bagasse for ethanol production. *Renewable energy* **2010,** *35,* 1130-1134.

Appendix A: Rotameter calibration

The Cole-parmer n082-03 rotameters used in the production of carbon nanotubes were supplied with calibration data for air at 1 atm and 21^{o}C. Thus corrections had to be performed to account for atmospheric pressure in Johannesburg of 0.81 atm, although no temperature correction was necessary. Further correction was required dependent on the gas being measured, hydrogen, argon or acetylene. The correction was performed using Equation A1, where F is the corrected flowrate, F' is the uncorrected flowrate, C is the gas correction factor, P is the atmospheric pressure and P' is the atmospheric pressure of the calibration. The Gas correction factors supplied by Cole-parmer are given in Table A1. The corrected calibration data are shown in Table A2.

$$F = C \left(\frac{P}{P'}\right)^{0.5} F' \qquad \text{A1}$$

Table A1: Gas correction factors supplied by Cole-parmer

Gas	Correction factor
Air	1
Argon	0.85
Acetylene	1.04
Hydrogen	3.61

Table A2: Calibration data for Cole-parmer n082-03 rotameter using a glass float

Scale reading	Air at 1atm & 21°C ml/min	Hydrogen (Johannesburg) ml/min	Argon (Johannesburg) ml/min	Acetylene (Johannesburg) ml/min
0	0	0	0	0
10	70	228.020	53.689	65.690
20	181	589.596	138.824	169.855
30	248	807.844	190.212	232.730
40	278	905.567	213.222	260.883
50	308	1003.290	236.231	289.036
60	370	1205.251	283.784	347.219
70	433	1410.469	332.105	406.340
80	487	1586.371	373.522	457.015
90	540	1759.015	414.172	506.752
100	594	1934.916	455.589	557.427
110	651	2120.590	499.308	610.918
120	699	2276.947	536.123	655.962
130	747	2433.304	572.938	701.007
140	794	2586.404	608.987	745.113
150	844	2749.275	647.336	792.035

Appendix B: Yeast information

FERMENTIS
Division of S.I.Lesaffre

Safale S-04
Dry ale yeast

Ingredients:	Yeast (Saccharomyces cerevisiae), rehydrating agent
Properties:	A well-known, commercial English ale yeast, selected for its fast fermentation character and its ability to form a very compact sediment at the end of the fermentation, helping to improve beer clarity. This yeast is recommended for the production of a large range of ale beers and is specially well adapted to cask-conditioned ales and fermentation in cylindro-conical tanks. Sedimentation: high. Final gravity: medium.
Dosage:	50 g/hl to 80 g/hl.
Pitching instructions:	Re-hydrate the dry yeast into yeast cream in a stirred vessel prior to pitching. Sprinkle the dry yeast in 10 times its own weight of sterile water or wort at 27C ± 3C. Once the expected weight of dry yeast is reconstituted into cream by this method (this takes about 15 to 30 minutes), maintain a gentle stirring for another 30 minutes. Then pitch the resultant cream into the fermentation vessel. Alternatively, pitch dry yeast directly in the fermentation vessel providing the temperature of the wort is above 20C. Progressively sprinkle the dry yeast into the wort ensuring the yeast covers all the surface of wort available in order to avoid clumps. Leave for 30 minutes and then mix the wort e.g. using aeration.
Fermentation temperature:	Recommended fermentation temperature: 15C – 24C.
Packaging:	4 display units each 38 x 11.5g nitrogen-flushed sachets in cardboard box.
Storage:	Store in cool (< 10C), dry conditions. Opened sachets must be sealed and stored at 4C and used within 7 days of opening. Do not use soft or damaged sachets.
Shelf life:	Refer to best before end date on sachets. 24 months from production date under recommended storage conditions.
Typical analysis:	% dry weight: 94.0 – 96.5 Viable cells at packaging: > 6 x 10^9 / gramme Total bacteria*: < 5 / ml Acetic acid bacteria*: < 1 / ml Lactobacillus*: < 1 / ml Pediococcus*: < 1 / ml Wild yeast non Saccharomyces*: < 1 / ml Pathogenic micro-organisms: in accordance with regulation **when dry yeast is pitched at 100 g/hl* *i.e. > 6 x 10^6 viable cells / ml*
Important notice:	Please note that any change to a fermentation process may alter the final product quality. We therefore advise that fermentation trials are carried out prior to using our yeast commercially.

Figure B1: Information sheet for Fermentis S-04 dried yeast

Appendix C: HPLC analysis

High performance liquid chromatography was carried out using a 1200 series Agilent HPLC. The HPLC was oppperated using a 0.0001 M solution of H_2SO_4 as the mobile phase at a flowrate of 0.8 ml min, a Bio-rad Fermentation Monitoring Column at 60^{o}C and a RID detector at 35^{o}C. The chromatographs were analysed using chemsoft software. The analysis was calibrated using two standard solutions: the first containing glucose, glycerol and ethanol, and the second containing maltose and fructose. 4 calibration points were made for each compound using dilutions of the standards. Chromatographs for the standards are shown in Figures C1 and C2. 4 known concentrations of each compound were analysed and used to form a linear calibration curve for each compound using the software. The results of the calibration are shown in Table C1, with the retention time denoting the elution time, the response factor denoting the amount of compound per unit area. The results of the HPLC analysis are given in Tables C2, C3, C4 and C5.

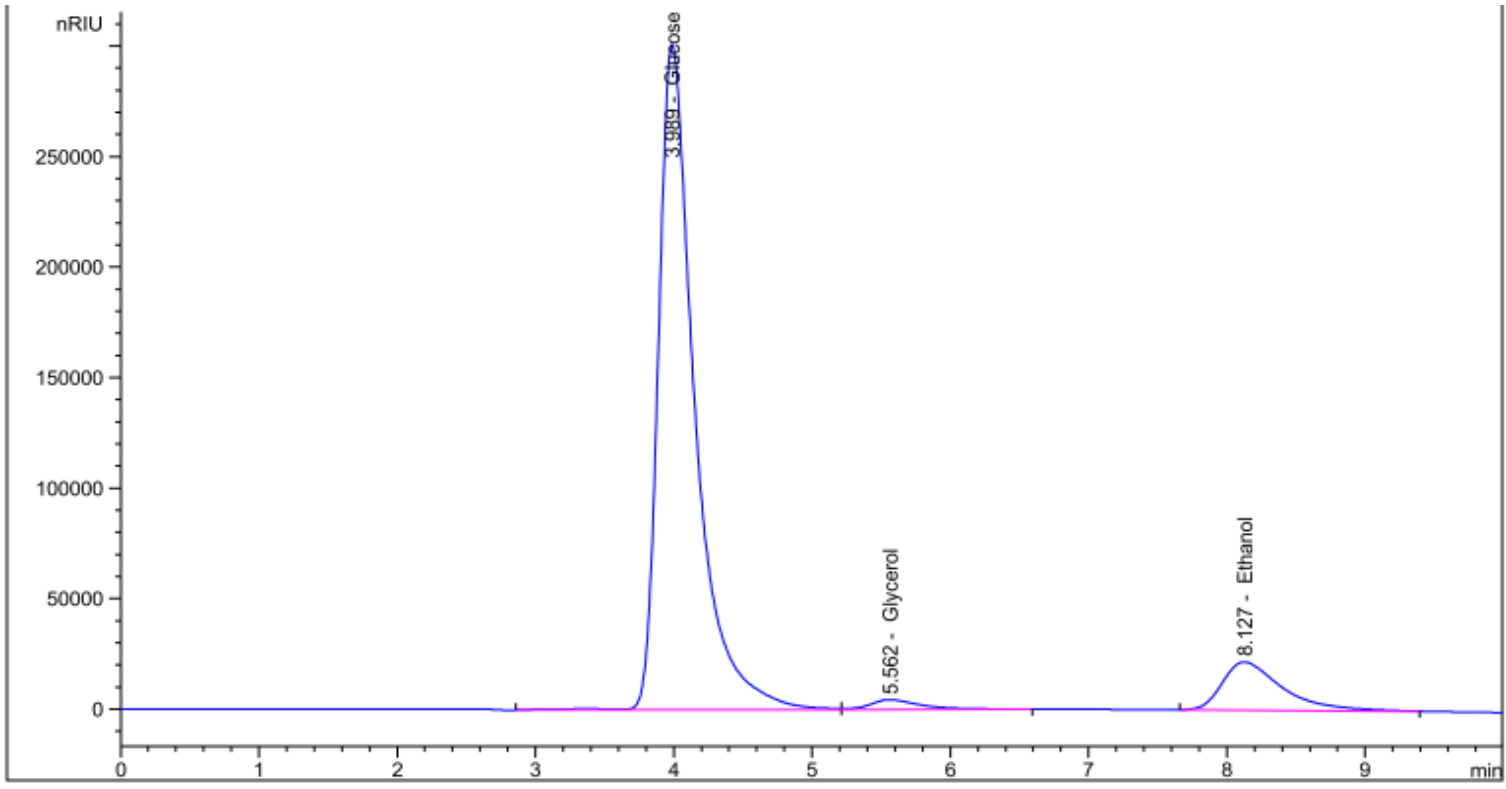

Figure C1: Chromatogram showing standard solution of glucose, glycerol and ethanol

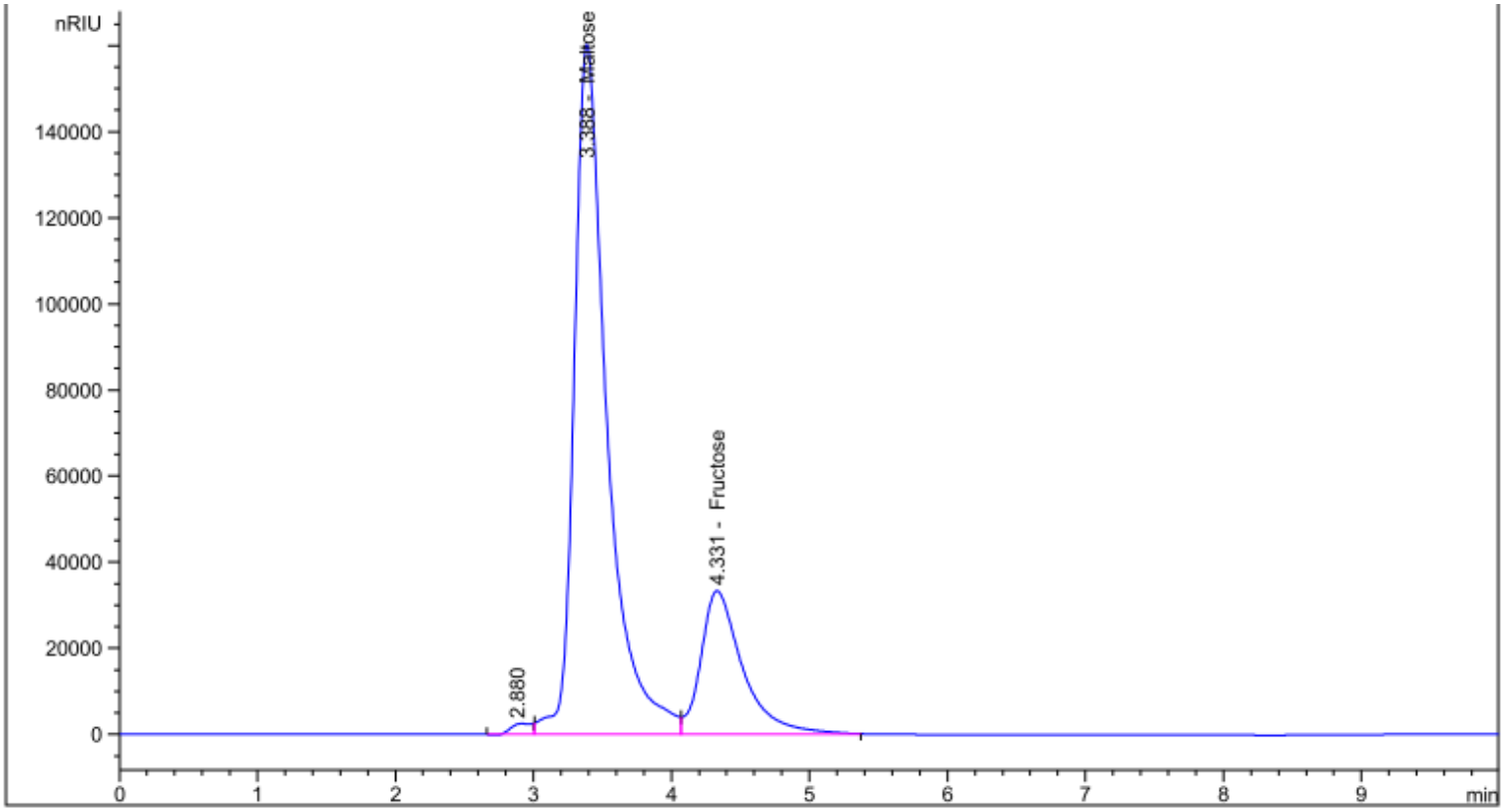

Figure C2: Chromatogram showing standard solution of maltose and fructose

Table C1: Calibration data for HPLC

Compound	Retention time (min)	Response factor (Amnt/area)
Maltose	3.388	$9.79264*10^{-6}$
Glucose	3.984	$9.20367*10^{-6}$
Fructose	4.331	$9.02542*10^{-6}$
Glycerol	5.562	$1.07737*10^{-5}$
Ethanol	8.120	$2.24800*10^{-5}$

Table C2: Results for HPLC analysis of fermentation using an initial yeast concentration of 1.93 g/l with carbon nanotube coated wire

Time hours	Maltose g/l	Glucose g/l	Fructose g/l	Glycerol g/l	Ethanol g/l
0.000	48.500	11.633	4.862	0.000	0.000
2.667	48.777	11.569	5.705	0.000	0.000
3.833	48.900	11.250	5.663	0.000	0.000
9.667	47.528	1.850	2.965	0.415	5.225
22.167	41.648	0.000	0.000	0.693	9.444
25.833	27.681	0.000	0.000	1.191	14.478
28.833	0.000	0.000	0.000	1.554	21.708
34.250	0.000	0.000	0.000	1.641	26.639
39.500	3.918	0.000	0.000	1.692	29.010

Table C3: Results for HPLC analysis of fermentation using an initial yeast concentration of 1.09 g/l with carbon nanotube coated wire

Time hours	Maltose g/l	Glucose g/l	Fructose g/l	Glycerol g/l	Ethanol g/l
0.000	49.056	15.869	0.000	0.000	0.000
2.667	43.021	10.119	4.962	0.000	0.000
3.833	48.886	11.511	5.700	0.000	0.000
9.667	48.332	5.697	3.334	0.000	3.028
22.167	51.569	0.000	0.000	0.554	5.922
25.833	38.172	0.000	0.000	0.856	10.498
28.833	11.580	0.000	0.000	1.280	17.775
34.250	0.000	0.000	0.000	1.293	23.125
39.500	3.166	0.000	0.000	1.226	28.159

Table C4: Results for HPLC analysis of fermentation using an initial yeast concentration of 0.51 g/l with carbon nanotube coated wire

Time hours	Maltose g/l	Glucose g/l	Fructose g/l	Glycerol g/l	Ethanol g/l
0.000	50.187	15.698	0.000	0.000	0.000
2.667	48.095	16.021	0.000	0.000	0.000
3.833	49.523	11.702	5.708	0.000	0.000
9.667	49.040	8.634	5.116	0.000	1.520
22.167	49.252	4.320	3.706	0.372	3.882
25.833	48.705	0.000	0.000	0.480	7.402
28.833	26.178	0.000	0.000	0.842	14.780
34.250	0.000	0.000	0.000	0.843	22.557
39.500	3.201	0.000	0.000	0.876	28.264

Table C5: Results for HPLC analysis of fermentation using an initial yeast concentration of 0.51 g/l with stainless steel wire

Time hours	Maltose g/l	Glucose g/l	Fructose g/l	Glycerol g/l	Ethanol g/l
0.000	49.875	15.850	0.000	0.000	0.000
2.667	49.070	16.354	0.000	0.000	0.000
3.833	49.525	11.584	5.854	0.000	0.000
9.667	49.873	8.877	5.369	0.000	1.381
22.167	48.800	4.753	3.190	0.000	3.748
25.833	47.365	0.000	2.219	0.435	7.124
28.833	28.163	0.000	0.000	0.812	14.798
34.250	0.000	0.000	0.000	0.934	21.051
39.500	3.281	0.000	0.000	0.840	28.342

Appendix D: Absorbance measurements

Absorbance measurements were performed to determine the yeast cell concentration during fermentation. Firstly experiments were carried out to determine the wavelength at which maximum absorbance occurs. This was tested using dried yeast in distilled water, and the absorbance was measured at various wavelengths. Figure D1 shows that the maximum absorbance occurs at 390 nm.

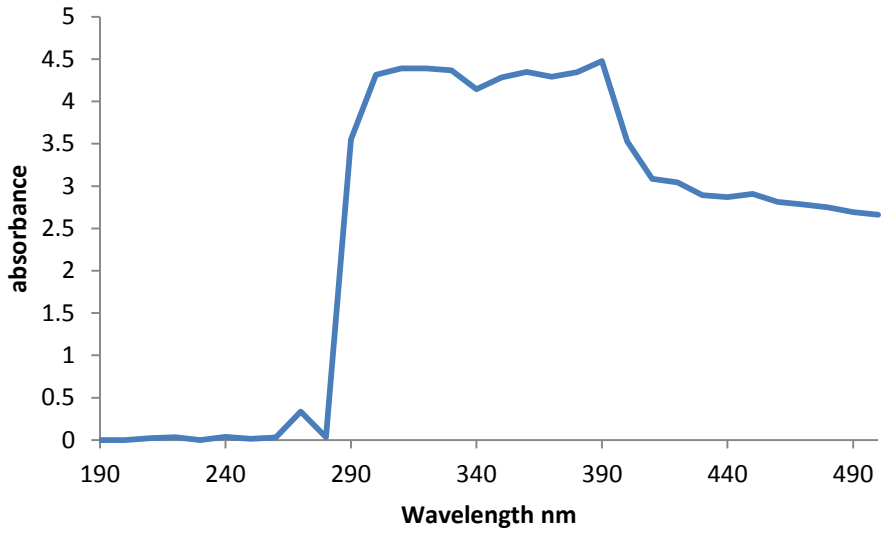

Figure D1: Absorbance of yeast at various wavelengths

The calibration curve for the absorbance readings was determined using known concentrations of yeast in malt extract solution. The dried yeast was rehydrated in distilled water and then inoculated into the malt extract solution. The concentration of yeast in the distilled water solution was determined by filtering the yeast cells from the solution. The filter disk was then dried at 80^{o}C for 4 hours. The mass of the filter disk was measured before filtration and after drying to determine the concentration of yeast cells in the solution. The points for the known concentration of yeast cells were then used to make a calibration curve through curve fitting a linear calibration. The calibration curve is shown in Figure D2. The calibration showed the relationship between yeast concentration and absorbance given in Equation D1, where y is the yeast cell concentration in g/l and x is the absorbance.

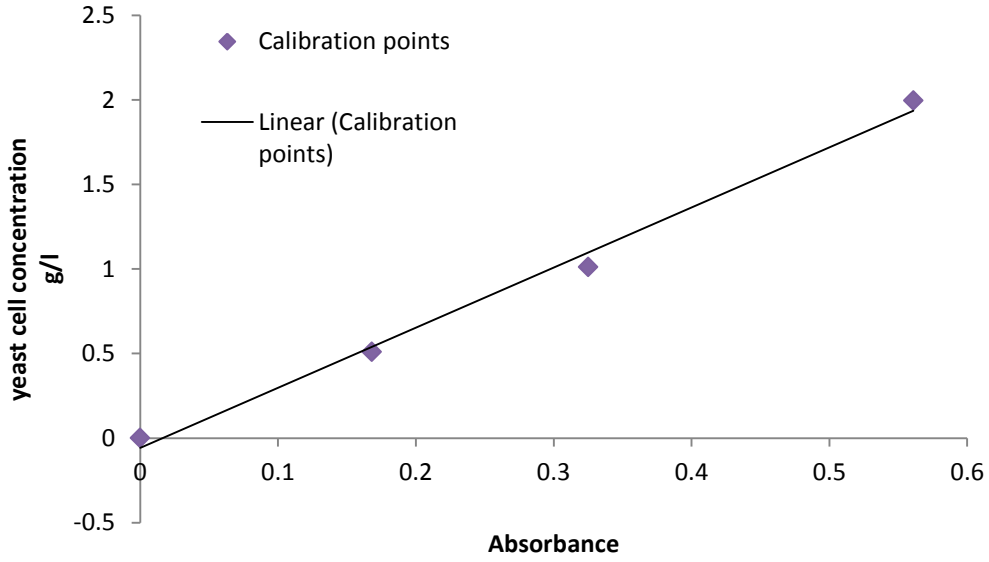

Figure D2: Calibration curve for finding yeast concentration

$$y = 3.5558x - 0.0578 \qquad \text{D1}$$

The calibration curve was used to determine the yeast cell concentrations for the fermentations these are given in Table D1

Table D1: Absorbance readings taken during fermentation

time hours	Absorbance: Initial yeast concentration 1.91 g/l with CNT wires	Absorbance: Initial yeast concentration 1.01 g/l with CNT wires	Absorbance: Initial yeast concentration 0.51 g/l with CNT wires	Absorbance: Initial yeast concentration 0.57 g/l with SS wires
0.000	0.561	0.325	0.177	0.159
2.667	0.576	0.359	0.123	0.145
3.833	0.646	0.319	0.226	0.180
9.667	0.540	0.310	0.203	0.195
22.167	1.007	0.702	0.432	0.445
25.833	1.250	0.972	0.602	0.458
28.833	1.258	1.094	0.985	0.909
34.250	0.190	0.692	1.255	1.266
39.500	0.288	0.094	0.229	0.201